scientific reports



OPEN

A comprehensive experimental and theoretical perspective of novel triazole-based pyridine and quinoline derivatives for corrosion protection of carbon steel in sulfuric acid solution

Kamelia Belal^{1,2}, A. H. El-Askalany¹, Eslam A. Ghaith^{1,3} & Ahmed Fathi Salem Molouk^{1,2,3⊠}

Herein, we synthesized two novel triazole compounds (KB1 and KB2). Their efficiency in inhibiting corrosion of carbon steel (CS) in 0.5 M H₂SO₄ was evaluated using open circuit potential (OCP) vs. time, potentiodynamic polarization (PP), electrochemical impedance spectroscopy (EIS), surface characterization methods, and computational studies. Based on EIS, the corrosion protection capacities of KB1 and KB2 increased with increasing concentration, reaching 86.9% and 92.4% at 9×10^{-5} M at 298 K for KB1 and KB2, respectively, which are consistent with the findings obtained viaPP. The PP curves imply that KB1 and KB2 act as mixed-type inhibitors. Meanwhile, their adsorption on the surface of CS obeyed the Langmuir isotherm. Using EIS and PP approaches, the effect of temperature on corrosion behavior was examined. As the temperature increased from 298 to 318 K, the efficacy of the inhibitors improved, then decreased at 328 K. This suggests that KB1 and KB2 may desorb from the CS at 328 K. The activation and adsorption parameters were computed and discussed. The effect of immersion time on CS corrosion was documented. The R_{ct} values of the KB2 compound peaked at 2770.0 Ω cm² after 6 h of immersion, later declining to 2685.0 Ω cm² after 93 h, thus evidencing the enhanced stability of the inhibitor's protective layer on the CS surface. Additionally, the steel surface was found to be positively charged in the H2SO4 solution, as indicated by the potential of zero charge (PZC) measurements using EIS. Surface morphology analysis using Atomic force microscopy (AFM), X-ray photoelectron spectroscopy (XPS), and Fourier transform infrared spectroscopy (FT-IR) demonstrated the formation of a protective layer with a high degree of coverage at 9×10^{-5} M. The test solutions were analyzed via UV-visible spectroscopy to determine whether complex formation between inhibitor molecules and Fe²⁺ ions is possible. The mechanism of inhibition was better understood via quantum chemical indices (based on DFT). The configurational adsorption performance of KB1 and KB2 on the Fe (110) surface was investigated viα Monte Carlo (MC) simulation, which revealed that inhibitors adsorbed on the Fe surface in a flat orientation. These results are thought to have some bearing on the sensible development of potent inhibitors for acidic corrosion.

Carbon steel (CS) is the primary material used in construction and structural applications for producing various industrial tools, including those for oil and water pipelines, power plants, etc¹. It is valued for its high strength, widespread availability, affordability, and ease of welding. However, despite these benefits, CS is prone to corrosion when subjected to aggressive solutions, causing significant financial losses². Sulfuric acid is a strong oxidizer and a dehydrator. It interacts violently with water and can ignite other materials. It is, therefore, categorized as a hazardous material, requiring safe transportation and storage to avoid any mishaps³. It is the most used acidic solution in industrial applications to eliminate oxides produced by chemical processes in steel and oil refineries. These acid solutions can harm metals used to build storage tanks and pipelines as time passes⁴.

¹Department of Chemistry, Faculty of Science, Mansoura University, Mansoura 35516, Egypt. ²Faculty of Science, Mansoura University Sustainable Energy Research Lab (MSER), Mansoura University, Mansoura 35516, Egypt. ³Faculty of Science, New Mansoura University, New Mansoura City, Egypt. [∞]email: molouk82@mans.edu.eg

One of the most popular and extensively used corrosion control strategies in a wide range of industries is the implementation of corrosion inhibitors, which are a flexible and effective method of reducing corrosion⁵⁻¹². Corrosion inhibitors are organic or inorganic compounds introduced in trace amounts to a corrosive medium and impede the anodic and/or cathodic metal corrosion reactions^{13,14}. Due to their high adsorption efficiency, environmental friendliness, and adjustable chemical structures, organic corrosion inhibitors have garnered increasing interest in recent years. Thanks to developments in molecular design, inhibitors with heteroatoms (N, O, and S) and numerous adsorption sites may now be synthesized, improving their capacity to create durable protective films on metal surfaces. Adsorption can occur chemically (chemisorption), physically (physisorption), or a combination of both¹⁵. Recent research has confirmed the adaptability of organic inhibitors in practical applications by demonstrating their efficiency under various corrosive conditions 16-28. These results are consistent with the current study's approach and encourage further investigation of novel hybrid inhibitors with enhanced adsorption capacities and sustainability profiles. Significantly, nitrogen-containing heterocyclic compounds, like triazole derivatives, have been widely researched for their chemical and biological characteristics and are commonly utilized in medicinal chemistry. Apart from their biological roles, they are acknowledged for their potency in impeding corrosion in acidic conditions^{29–34}. Triazoles are five-membered heterocyclic compounds containing three nitrogen atoms with lone pairs and π -electrons, which are strongly adsorbed on metal surfaces. Nearby heteroatoms (N-N) improve adsorption on the metal surfaces³⁵. Additionally, their application in the pharmaceutical sector demonstrated their non-hazardous qualities³⁶. Based on previous studies, compounds containing pyridine and quinoline have strong corrosion-inhibiting properties^{37–42}. The significance of choosing the tested inhibitors as corrosion inhibitors lies in their economic feasibility and the presence of an electronrich system, such as an aromatic ring and heteroatoms 43,44. By establishing coordination bonds with the metal surface, these atoms can produce a protective layer that lessens corrosion. Moreover, they can be used in practical applications because their synthesis is economical and environmentally friendly. Consequently, the innovation of selecting these inhibitors is the cost-effective molecular design that combines three extremely potent moieties into one inhibitor molecule: hydrazinyl triazole, clubbed pyridine/ quinoline. These moieties are well-known for their potent electron-donating capabilities and potential to create coordination bonds with metal surfaces. Combining them results in a structure with more adsorption sites, higher electron density, and better surface contact, all boosting corrosion inhibition performance. Moreover, the compounds were synthesized via an environmentally friendly ultrasound-assisted method. Since corrosion inhibition literature has not yet documented this design in conjunction with an ultrasound-assisted green synthesis method, it provides a novel and sustainable approach. As a result, we assessed the ability of (Z)-4-amino-5-(2-(pyridin-4-ylmethylene)hydrazinyl)-4H-1,2,4-triazole-3-thiol (KB1) and (Z)-4-amino-5-(2-((2-azidoquinolin-3-yl) methylene)hydrazinyl)-4H-1,2,4-triazole-3-thiol (KB2) to impede the dissolution of CS in 0.5 M H₂SO₄ utilizing electrochemical techniques. The CS's surface morphology, composition, and structure were determined using various characterization techniques: AFM, XPS, and FT-IR. The test solutions were analyzed via UV-Visible spectroscopy to check the complex formed among ferrous ions and the investigated inhibitors. Additionally, computational studies via quantum calculations (DFT) and Monte Carlo (MC) simulations are conducted to reinforce the experimental outcomes.

Experimental techniques Working electrode preparation

The utilized CS sheet has the following compositions (weight%): C 0.2%, Si 0.25%, S 0.05%, Mn 0.5%, and Fe 99%. It was sliced into 1 cm x 1 cm pieces and firmly cemented in an epoxy/hardener mixture. This guaranteed that the coupon used in the electrochemical measurements would have an exposed area of 1 cm². Before testing, the working electrode was polished using a series of emery paper grades (320, 400, 1000, and 2000) to achieve a mirror surface, cleaned with double-distilled water, and dehydrated with filter papers.

General procedure for the synthesis of inhibitors

As indicated in Fig. 1, a mixture of 4-amino-5-hydrazineyl-4H-1,2,4-triazole-3-thiol (1) (0.146 g,1 mmol) and pyridine-4-carboxaldehyde (2) (0.094 mL, 1 mmol) or 2-azidoquinoline-3-carbaldehyde (3) (0.198 g, 1 mmol) was mixed and irradiated under ultrasound for 3 min at ambient temperature in MeOH (20 mL) containing 3 drops of conc. H_2SO_4 as a catalyst. The formed precipitates (KB1 and KB2) were filtered off and washed with hot MeOH. Figures \$1–\$6 in the supplementary file display the 1 HNMR, 1 3CNMR, and mass spectra, while Table \$1 presents further details of the synthesis process of the inhibitors.

(*Z*)-4-amino-5-(2-(pyridin-4-ylmethylene)hydrazinyl)-4*H*-1,2,4-triazole-3-thiol (KB1). Yield, 92%; orange powder; m.p 244–245 °C. IR ($\nu_{\rm max}$, cm⁻¹): 3439 (NH₂), 3266 (NH), 3084 (sp² CH), 1622, 1618, 1577, 1557 (C = N & C = C). ¹HNMR (DMSO- d_6 , 500 M*Hz*): δ (ppm) 5.57 (s, 2 H, NH₂), 7.84 (d, J = 6.5 *Hz*, 2 H), 8.34 (s, 1 H, CH),

Fig. 1. Synthesis of inhibitors.

8.69 (d, J=6 Hz, 2 H), 11.51 (s, 1 H, NH), 13.15 (s, 1 H, SH). 13 CNMR (DMSO- d_{e^2} 125 MHz): δ (ppm) 121.62 (2 C), 139.38, 146.08 (2 C), 146.43, 149.00, 164.99.)EMIS) m/z (%): 235.71 (M $^+$, 44.25%), 191.80 (90.74%), 145.14 (100%, base peak), 114.83 (63.39%), 104.17 (63.56%), 95.92 (55. 72%), 94.70 (89.00%), 62.30 (58.22%). (Z)-4-amino-5-(2-((2-azidoquinolin-3-yl)methylene)hydrazinyl)-4H-1,2,4-triazole-3-thiol (KB2). Yield,

(Z)-4-amino-5-(2-((2-azidoquinolin-3-yl)methylene)hydrazinyl)-4*H*-1,2,4-triazole-3-thiol (KB2). Yield, 91%; brown powder; m.p 238–239 °C. IR (v_{max} , cm⁻¹): 3415 (NH₂), 3292 (NH), 3035) sp² CH), 1674, 1641, 1614, 1547 (C=N & C=C). ¹HNMR (DMSO- d_6 , 400 M*Hz*): δ (ppm) 3.55–3.67 (br, 2 H, NH₂), 7.82 (t, *J*=7.4 *Hz*, 1 H), 7.97 (t, *J*=7.8 *Hz*, 1 H), 8.36 (d, *J*=8 *Hz*, 1 H), 8.57 (s, 1 H, CH), 8.61 (d, *J*=8.4 *Hz*, 1 H), 8.93 (s, 1 H, CH), 11.48 (s, 1 H, NH), 13.16 (s, 1 H, SH). ¹³CNMR (DMSO- d_6 , 100 M*Hz*): δ (ppm) 116.65, 120.51, 124.47, 127.84, 128.84, 130.16, 130.55, 131.92, 136.67, 146.76, 149.62, 165.11.)EMIS) m/z (%): 326.69 (M⁺, 23.26%), 242.34 (100%, base peak), 211.52 (67.21%), 206.05 (63.55%), 127.03 (96.45%), 121.16 (81.45%), 109.90 (68.40%), 76.99 (92.30%).

Solutions

The corrosive medium, $0.5~\mathrm{M}~\mathrm{H}_2\mathrm{SO}_4$, was prepared by diluting the AR-grade sulfuric acid solution with double-distilled water. Economic and practical considerations were the key factors in selecting the tested inhibitors' concentrations. It would be ineffective to use concentration over the saturation point, and doing so might result in needless expenses and possible environmental issues. To ensure efficient corrosion prevention while maintaining cost-effectiveness and minimizing excessive chemical use, the tested concentrations were selected. Therefore, stock solutions of the tested inhibitors ($10^{-3}~\mathrm{M}$) were prepared. Dimethyl sulfoxide ($10~\mathrm{mL}$) was used to dissolve the calculated amount of inhibitor, and it was then brought to $100~\mathrm{mL}$ with absolute ethanol. Different concentrations of the investigated inhibitors ($1-9\times10^{-5}~\mathrm{M}$) were employed by dilution from the stock solution. The percentage of solvents in which the inhibitor dissolved was maintained throughout the prepared solutions, both with and without the inhibitors, to prevent the effect of solvents on the inhibition. No precipitation or turbidity was observed throughout the experiments, indicating good solubility and stability of the inhibitors in the test solutions.

Electrochemical measurements

Electrochemical tests were carried out in a corrosion cell using three electrodes: a CS working electrode, a platinum wire as the counter electrode, and a saturated calomel electrode (SCE) as the reference electrode. The three electrodes were immersed in the test solutions for 35 min before each experiment to achieve a stabilized OCP. EIS measurements were performed using AC signals of 10 mV amplitude at OCP and the frequency range from 100 kHz to 0.1 Hz. The PP measurements were achieved by sweeping the potential from –500 mV to 500 mV against OCP using a scan rate of 0.5 mV/s. All experiments were performed with newly prepared solutions at 298 K *via* a Potentiostat/Galvanostatic/ZRA analyzer (Gamry 5000E, USA). At each inhibitor concentration, the experiments were repeated three times to ensure reproducibility and accuracy of the corrosion inhibition results.

Zero charge potential

EIS was implemented to estimate the potential of zero charge (PZC). It was carried out at various potentials with an AC amplitude of 10 mV in 0.5 M $\rm H_2SO_4$ solutions with $\rm 5 \times 10^{-5}$ M of KB1 and KB2. A plot has been created to show how the applied voltage affects the variation of $\rm C_{dl}$. $\rm E_{PZC}$ represents the lowest $\rm C_{dl}$ value.

Surface characterization

CS specimens were polished with different grades of emery papers, washed, dried, and exposed to $0.5~\mathrm{M}$ H $_2\mathrm{SO}_4$ solution without and with adding $9\times10^{-5}~\mathrm{M}$ of KB1 and KB2 for 24 h, after that the specimens were brought out and dried to analyze the morphology via Nanosurf FlexAFM 3, Gräubernstrasse 12, 4410 Liestal, Switzerland for AFM analysis and the components of the film that developed on the CS was investigated via AXIX Ultra DLD, Kratos, UK for XPS analysis. FTIR analysis detects the functional groups present in the inhibitor and provides qualitative insight into the inhibitor's adsorption onto the CS surface.

UV-Visible spectra

Corrosion protection was examined by UV-Visible spectrophotometry both before and after the CS coupons were submerged for 48 h to gather additional information on the complex formed between Fe^{2+} ions and the tested inhibitors. The spectra were recorded *via* a T80+UV/vis spectrometer (UK).

Theoretical computations

The energy minimization of KB1 and KB2 in an aqueous medium was investigated through DFT calculations using the GGA method with BOP functional and the DNP basis set in the Dmol³ module of BIOVIA Materials Studio 2017 software ^{45,46}. Based on DFT calculations, several quantum indices were calculated ⁴⁷. The Adsorption Locator module was also applied for the MC simulation ⁴⁸. Following the use of the COMPASS force field to optimize the geometry of both the tested molecules and Fe (1 1 0), the Adsorption Locator module uses Monte Carlo searches to determine the feasible adsorption configurations of the inhibitors on the surface and their influence on the inhibitory performance ⁴⁹.

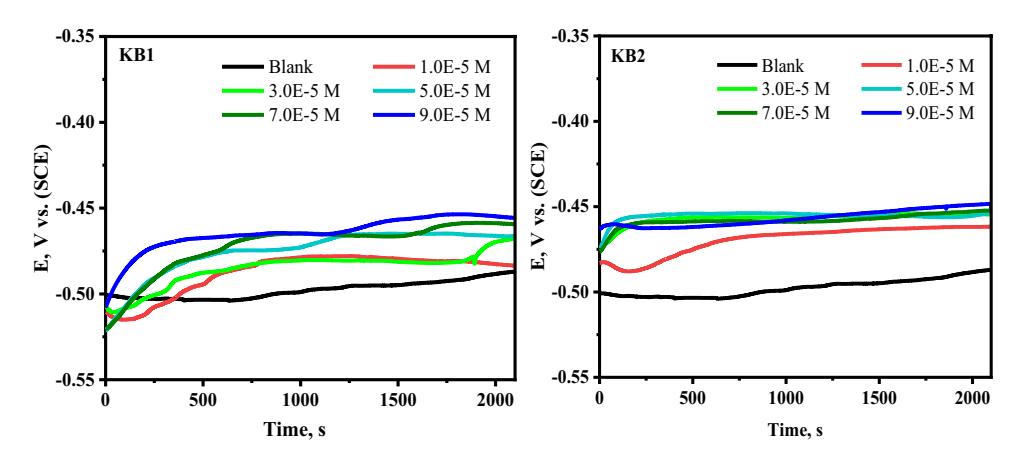


Fig. 2. OCP-time curves for CS submerged in 0.5 M $\rm H_2SO_4$ before and after varying doses of KB1 and KB2 at 298 K.

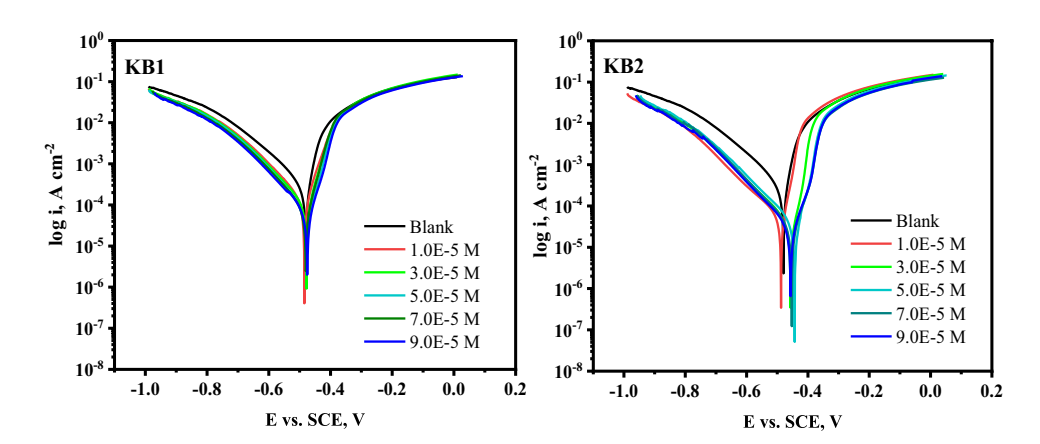


Fig. 3. Tafel diagrams for CS in 0.5 M H₂SO₄, both without and with KB1 and KB2 at 298 K.

Inhibitors	Conc. (M)	-E _{corr} , mV vs. SCE	i _{corr} · μA cm ⁻² ± SD	β _a , mVdec ⁻¹	β _c , mVdec ⁻¹	C.R., mpy	$R_p, \Omega \text{ cm}^2$	θ	%IE
Blank	0.5 M H ₂ SO ₄	480.0	327.0 ± 0.16	53.80	159.3	149.5	53.40	-	-
	1×10 ⁻⁵	483.0	120.0 ± 0.29	49.70	112.4	54.91	129.70	0.633	63.3
	3×10 ⁻⁵	478.0	93.20±0.16	44.60	110.7	42.56	148.12	0.715	71.5
KB1	5×10 ⁻⁵	467.0	82.10 ± 0.07	48.40	133.5	37.48	187.87	0.749	74.9
	7×10^{-5}	473.0	52.00 ± 0.15	38.00	66.80	23.76	202.26	0.841	84.1
	9×10 ⁻⁵	470.0	41.00 ± 0.04	41.70	63.60	18.73	266.74	0.875	87.5
	1×10 ⁻⁵	457.0	71.00 ± 0.73	75.00	155.8	32.43	309.63	0.783	78.3
	3×10 ⁻⁵	445.0	39.40 ± 0.41	42.80	141.7	17.98	362.27	0.880	88.0
KB2	5×10 ⁻⁵	452.0	31.80 ± 0.49	39.90	132.6	14.53	418.80	0.903	90.3
	7×10 ⁻⁵	459.0	29.30 ± 0.34	47.80	131.7	13.38	519.74	0.910	91.0
	9×10 ⁻⁵	458.0	28.20 ± 0.57	49.70	133.5	12.87	557.66	0.914	91.4

Table 1. Corrosion parameters based on extrapolation of CS Tafel curves at 298 K.

Results and discussion Open circuit potential (OCP)

The steady-state potential was measured by recording the change in OCP values after 35 min of exposure to $0.5~\mathrm{M}~\mathrm{H}_2\mathrm{SO}_4$, both without and with inhibitors at various concentrations (Fig. 2). After 10 min, the OCP curves become nearly linear. The presence of KB1 and KB2 caused the OCP curves to stabilize at more positive values, indicating the formation of a protective layer on the CS surface, primarily on the anodic sites 50,51 .

PP analysis

Tafel polarization graphs for CS in 0.5 M $\rm H_2SO_4$ at 298 K without and with different concentrations of KB1 and KB2 are displayed in Fig. 3. Table 1 provides the electrochemical parameters obtained from Tafel plots. Equation (1) was applied to find the inhibition effectiveness based on the i_{corr} values⁵².

$$\% \text{ IE} = \theta \times 100 = \left(1 - \frac{i_{corr}}{i^{\circ}_{corr}}\right) \times 100 \tag{1}$$

 i°_{corr} and i_{corr} correspond to the corrosion current densities before and after the addition of the inhibitor. It is evident from Table 1 that i_{corr} declines as the inhibitor's concentration rises, reaching the lowest corrosion rate value at 9×10^{-5} M. This phenomenon can be explained by the inhibitors adhering to the CS surface and establishing a protecting layer that shields the surface from the harsh environment, enhancing inhibition capacity values, which reached 87.5% and 91.4% for KB1 and KB2, respectively⁵³. The Tafel slopes (β_a , β_c) do not alter with varying doses of KB1 and KB2, suggesting that their addition has no effect on the corrosion mechanism and that the principal mechanism of inhibition is the adsorption of inhibitors onto the CS surface, which blocks its active sites⁵⁴. As seen from the E_{corr} values in Table 1, there is a shift (<85 mV) from the E_{corr} of the blank when inhibitor molecules are present. This implies that the substances being studied have mixed-type inhibitory effects⁵⁵. Additionally, using Eq. (2), the polarization resistances (R_p) for the CS/H₂SO₄ system at various concentrations of KB1 and KB2 were determined:

$$R_p = \frac{\beta \, a\beta \, c}{2.303(\beta \, a + \beta \, c)i_{\text{corr}}} \tag{2}$$

As the concentration rose, the R_p dramatically increased, indicating the formation of a protective film of KB1 and KB2 on the CS surface⁵⁶.

EIS measurements

EIS, a non-destructive technique, was used to investigate the interface of CS substrates with and without inhibitors. It provides valuable insights into the corrosion inhibition mechanisms by revealing the electro-

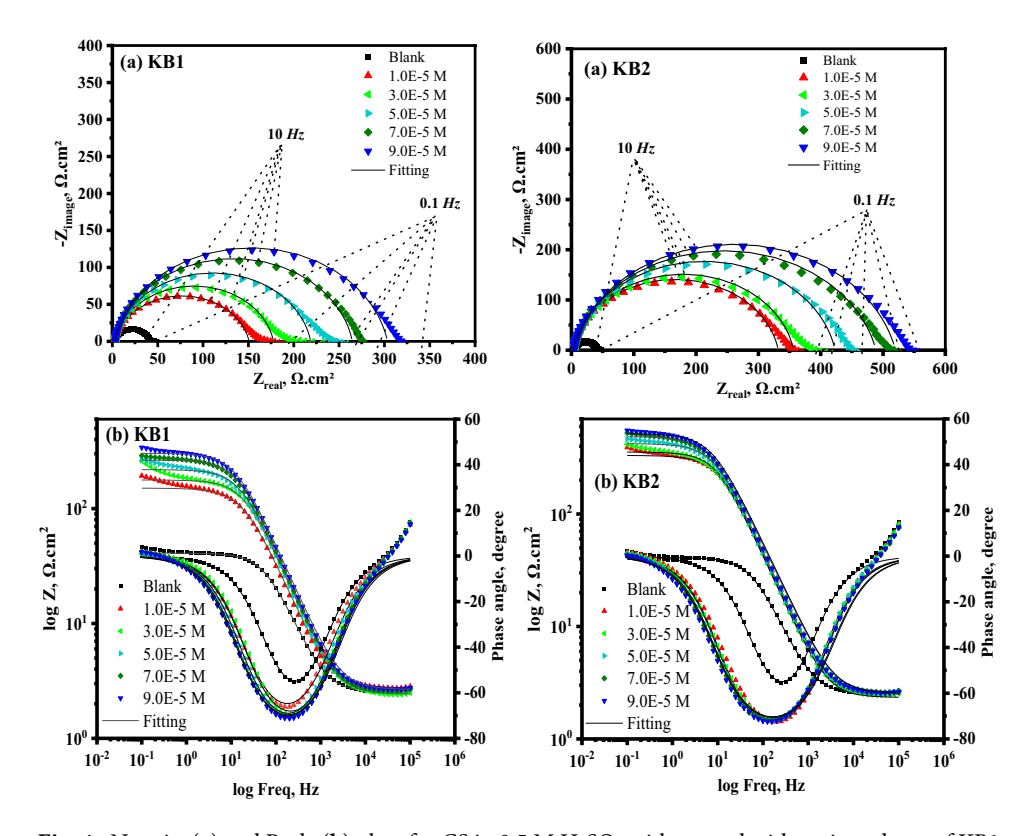


Fig. 4. Nyquist (a) and Bode (b) plots for CS in 0.5 M H_2SO_4 without and with various doses of KB1 and KB2 at 298 K.

Fig. 5. The applied equivalent electrical circuit for fitting EIS data.

Inhibitors	Conc. (M)	$R_{\rm s}$, Ω cm ²	$R_{\rm ct}$, Ω cm ² ± SD	Y_0 x10 ⁻⁶ , μΩ ⁻¹ s ⁿ cm ⁻²	n	C _{dl,} µF.cm ⁻²	Goodness of fit (x10 ⁻³)	θ	%IE
Blank	0.5 M H ₂ SO ₄	2.520	39.50 ± 0.24	125.1	0.907	72.4	3.732		
	1×10 ⁻⁵	2.744	148.0 ± 0.82	100.4	0.883	57.6	5.432	0.733	73.3
	3×10 ⁻⁵	2.423	175.2 ± 0.41	75.36	0.900	46.6	8.130	0.775	77.5
KB1	5×10 ⁻⁵	2.630	216.0 ± 0.16	72.19	0.902	46.0	4.991	0.817	81.7
	7×10 ⁻⁵	2.563	262.0 ± 0.33	68.16	0.900	43.6	4.089	0.849	84.9
	9×10 ⁻⁵	2.660	300.7 ± 0.41	66.25	0.891	40.9	4.109	0.733 0.775 0.817	86.9
	1×10 ⁻⁵	2.477	329.5 ± 0.53	70.81	0.900	46.7	4.828	0.880	88.0
	3×10 ⁻⁵	2.333	354.0 ± 0.61	68.93	0.901	45.7	4.535	0.888	88.8
KB2	5×10 ⁻⁵	2.543	420.6 ± 0.78	68.80	0.891	44.5	3.500	0.906	90.6
	7×10 ⁻⁵	2.574	486.1 ± 0.65	67.93	0.870	40.8	3.406	0.919	91.9
	9×10 ⁻⁵	2.541	517.4±0.57	65.20	0.871	39.4	3.341	0.924	92.4

Table 2. The parameters obtained from EIS for KB1 and KB2 at 298 K.

resistive and capacitive properties of the substrates under investigation 57 . The Nyquist and Bode diagrams of CS, produced in $0.5 \,\mathrm{M}\,\mathrm{H}_2\mathrm{SO}_4$ solution with and without different doses of KB1 and KB2 at 298 K, are displayed in Fig. 4a and b, respectively. As observed in Fig. 5, the acquired impedance values were fitted to a standard electrochemical circuit. Table 2 provides a summary of the evaluated corrosion parameters. Equation (3) can be utilized to get % IE based on the charge-transfer resistance (R_{ct}) values 58 :

$$\% \text{ IE} = \theta \times 100 = \left(1 - \frac{R^{\circ}_{ct}}{R_{ct}}\right) \times 100 \tag{3}$$

where " R_{ct}^{o} " represents the charge-transfer resistance in blank solution and " R_{ct} " represents the chargetransfer resistance using different doses of KB1 and KB2. Nyquist plots (Fig. 4a) clearly show that the spectra consist of a single capacitive semicircle, indicating that the charge transfer process primarily controls the dissolution of CS, and the adsorption of KB1 and KB2 is achieved by simple surface coverage. As opposed to the uninhibited solution, the capacitive semicircle size of CS significantly increased upon the addition of the different concentrations of KB1 and KB2, implying a decrease in the rate of CS corrosion and an increase in % IE⁵⁹. This means that the surface in the aggressive solution is protected *via* the developed adsorbed layer. The Bode graphs for KB1 and KB2 are displayed in Fig. 4b. Upon elevation of the inhibitor concentration, the impedance value rose; the higher impedance for KB2 suggests that it provides more safeguards for CS than KB1³⁴. Additionally, Nyquist plots deviate from idealized semicircles. This depression of the semicircles is attributed to many factors, including frequency dispersion effects, electrode surface irregularities, grain boundary impedance, and impurities 60. The values of R_{ct} (Table 2) increase from 39.50 Ω .cm² for uninhibited CS to 300.7 Ω .cm² and 517.4 Ω .cm² at 9×10^{-5} M of KB1 and KB2, respectively. The formation of thin layers of inhibitors at the CS-corrosive solution interface caused this observation⁶¹. As the concentrations of KB1 and KB2 rise, the double-layer capacitance (C_{dl}) values decrease, signifying that KB1 and KB2 molecules, which have lower dielectric constants, displace water molecules on the CS⁶². Analyzing C_{dl} data *via* the constant phase element (CPE) data parameters (\hat{Y}_0 and n) was achieved, whereas the CPE parameters for the circuit displayed in Fig. 5 were utilized to calculate C_{dl} via the following formula⁶³:

$$C_{dl} = \left(Y_0 R_{ct}^{(1-n)}\right)^{1/n}$$
 (4)

.

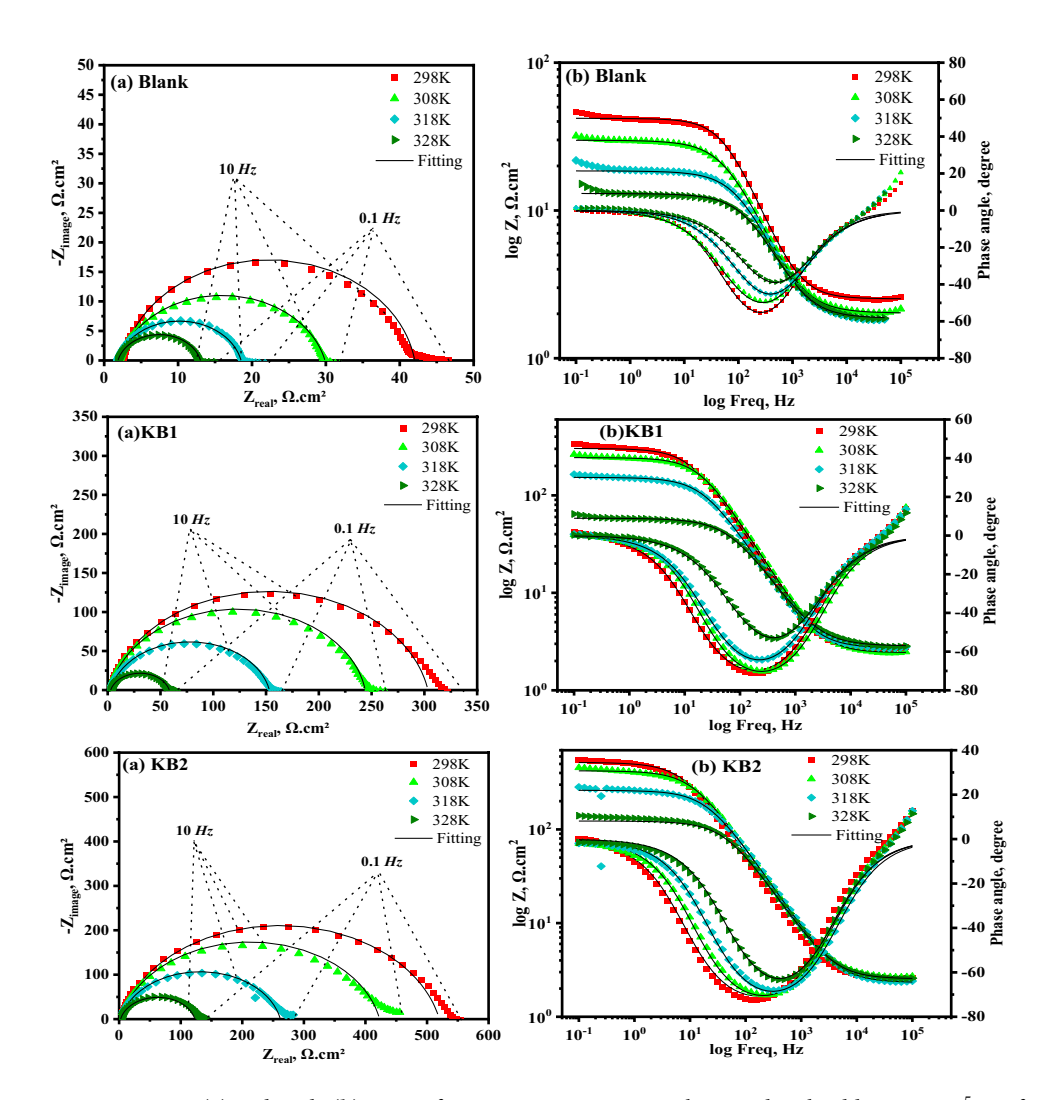


Fig. 6. Nyquist (a) and Bode (b) curves for CS in 0.5 M $\rm H_2SO_4$ without and with adding 9×10^{-5} M of KB1 and KB2 at different temperatures.

Temp, K	Compound	$R_{\rm s}$, Ω cm ²	$R_{\rm ct}$, Ω cm ² ± SD	Goodness of fit (x10 ⁻³)	θ	%IE
	Blank	2.520	39.50 ± 0.24	3.732	-	-
298	KB1	2.660	300.7 ± 0.41	4.109	0.869	86.9
	KB2	2.541	517.4±0.57	3.732 –	92.4	
	Blank	2.018	27.86 ± 0.85	6.548	-	-
308	KB1	2.428	241.5 ± 0.53	3.849	0.885	88.5
	KB2	2.609	241.5±0.53 3.849 0.88 420.3±0.61 3.581 0.93 16.70±0.57 2.737 -	0.934	93.4	
	Blank	1.825	16.70 ± 0.57	2.737	-	-
318	KB1	2.714	150.4±0.41	3.447	0.889	88.9
	KB2	2.316	259.4±0.69	5.030	0.936	93.6
	Blank	1.862	11.17 ± 0.80	2.663	-	-
328	KB1	2.841	55.46 ± 0.76	2.942	0.799	79.9
	KB2	2.532	120.4±0.86	3.022	- 0.869 0.924 - 0.885 0.934 - 0.889 0.936 - 0.799	90.7

Table 3. The parameters obtained from EIS in 0.5 M $\rm H_2SO_4$ before and after adding 9×10^{-5} M of KB1 and KB2 at various temperatures.

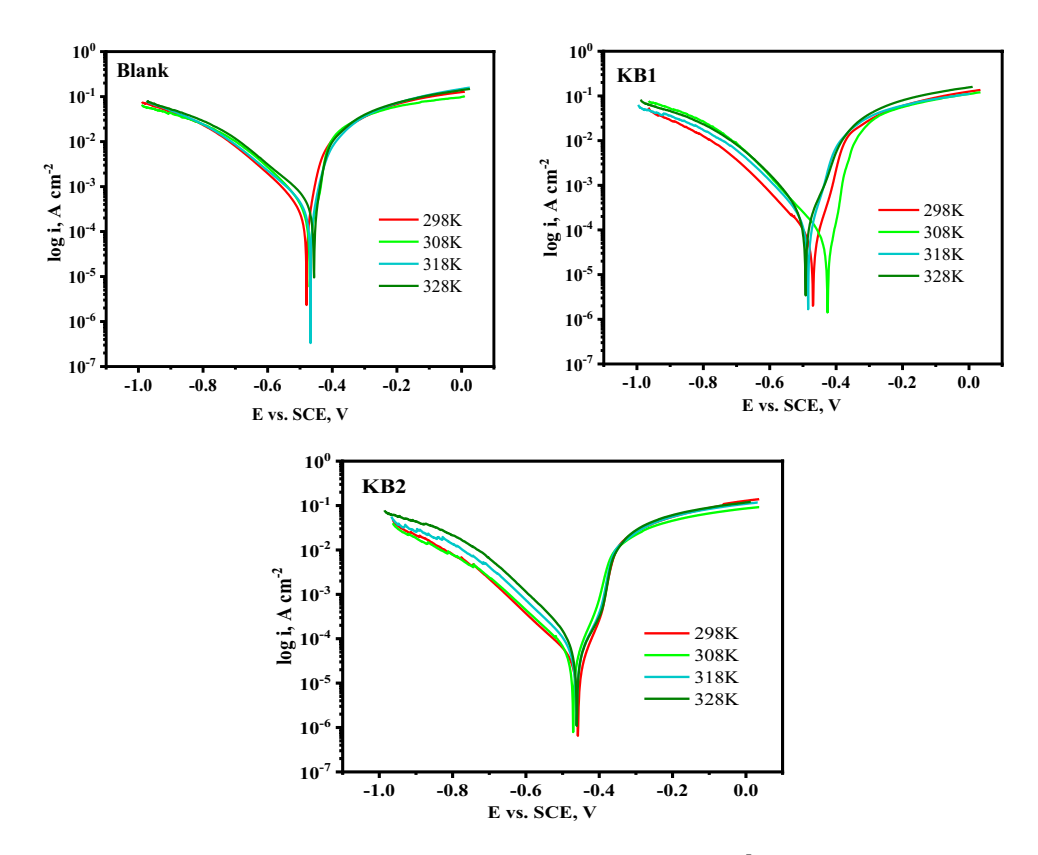


Fig. 7. PP curves for CS in 0.5 M $\rm H_2SO_4$ without and with adding 9×10^{-5} M of KB1 and KB2 at different temperatures.

Temp, K	Compound	-E _{corr} , mV vs. SCE	i _{corr} , μAcm ⁻² ± SD	C.R. mpy	θ	%IE
	Blank	480.0	327.0 ± 0.16	149.5	-	-
298	KB1	470.0	41.00 ± 0.04	18.73	0.875	87.5
	KB2	458.0	28.20 ± 0.57	12.87	-	91.4
	Blank	454.0	511.0 ± 0.89	233.4	-	-
308	KB1	457.0	61.10 ± 0.57	27.92	0.880	88.0
	KB2	475.0	39.10 ± 0.65	17.88	- 0.875 0.914 - 0.880 0.923 - 0.886 0.932 - 0.789	92.3
	Blank	467.0	717.0 ± 0.82	327.7	-	-
318	KB1	477.0	81.40 ± 0.61	37.19	0.886	88.6
	KB2	481.0	49.00 ± 0.89	22.39	- 0.875 0.914 - 0.880 0.923 - 0.886 0.932 - 0.789	93.2
	Blank	460.0	766.0 ± 0.78	349.8	-	-
328	KB1	492.0	162.0 ± 0.45	73.82	0.789	78.9
	KB2	480.0	71.10 ± 0.69	32.48	- 0.875 0.914 - 0.880 0.923 - 0.886 0.932 - 0.789	90.7

Table 4. The parameters obtained from PP in 0.5 M $\rm H_2SO_4$ before and after adding 9×10^{-5} M of KB1 and KB2 at various temperatures.

where the CPE exponent n, depends on the character of the CS surface, while \mathbf{Y}_0 is the CPE magnitude 64. The data collected using the PP approach is supported by the EIS findings.

Effect of temperature

The inhibition potency of KB1 and KB2 for the dissolution of CS in 0.5 M $\rm H_2SO_4$ in the absence and presence of the maximum concentration was evaluated at various temperature ranges (298–328 K) *via* EIS and PP measurements. Increased system temperature enhances the kinetic mobility of corrosive species. By decreasing the deposited corrosion products and even the adsorbed film covering the CS surface, this behavior exposes a larger area of the CS to the corrosive solution, which in turn enhances iron oxidation and $\rm H_2$ evolution⁶⁵. As

	Arrheniu	s	Transition state					
Compounds	Slope	$\mathbf{E_a^*}$, kJ mol $^{-1}$	Slope	Intercept	ΔH*, kJ mol ⁻¹	- ΔS*, J mol ⁻¹ K ⁻¹		
Blank	- 1237.3	23.69	- 1101.6	3.7695	21.09	125.39		
KB1	- 1862.7	35.66	- 1727	4.9092	33.07	103.57		
KB2	- 1271.5	24.35	- 1135.8	2.78441	21.75	144.26		

Table 5. Activation thermodynamic parameters for CS in the absence and presence of KB1 and KB2 at different temperatures.

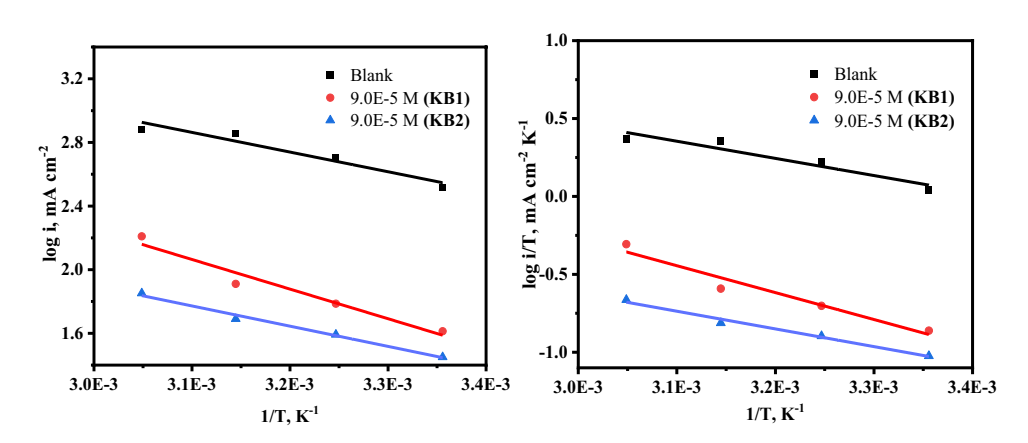


Fig. 8. Arrhenius (left) and transition state (right) plots for CS in 0.5 M $\rm H_2SO_4$ without and with 9×10^{-5} M of KB1 and KB2.

revealed in Fig. 6a, the Nyquist spectra of CS in 0.5 M H_2SO_4 without and with the addition of 9×10^{-5} M of KB1 and KB2 showed a semicircular shape that shrank in diameter as the temperature rose, suggesting that the mechanism underlying the CS corrosion process is independent of temperature. As the temperature rose, the data of % IE in Table 3 increased marginally, reaching 88.6% and 93.2% for KB1 and KB2, respectively. This demonstrated their capacity to inhibit and adsorb onto the surface of CS as a stable film over a range of temperatures, protecting it from the damaging effects of 0.5 M H₂SO₄ solution via chemical bonds (chemical adsorption)⁶⁶. At 328 K, the % IE values decreased, which indicates that higher temperatures (328 K) may have led to the desorption of KB1 and KB2 from the surface. The temperature effect caused a slight increase in corrosion. The Bode diagrams in Fig. 6b show a one-time constant at all temperatures, confirming the presence of a single capacitive loop. Increasing temperature decreases the impedance modulus values at lower frequencies for the systems under study (Fig. 6b)⁶⁴. PP measurements revealed similar findings, which are shown in Fig. 7 and Table 4. As temperature rises, so does the i_{corr} and the rate at which CS dissolves. Since the i_{corr} values obtained in the existence of KB1 and KB2 were lower than those achieved in their absence, it is evident that the investigated inhibitors significantly hindered the corrosion response of CS. The activation energy (E_a^*), change in enthalpy, and entropy (ΔH^* , ΔS^*) presented in Table 5 are thermodynamic activation parameters of the CS corrosion computed based on PP utilizing the Arrhenius and transition state equations as follows⁶⁷.

$$\log i_{corr} = -\frac{E_a^*}{2.303RT} + \log (A)$$
 (5)

$$\log\left(\frac{i_{\rm corr}}{T}\right) = \log\left(\frac{R}{Nh}\right) + \left(\frac{\triangle S^*}{2.303R}\right) - \left(\frac{\triangle H^*}{2.303RT}\right),\tag{6}$$

where the Arrhenius pre-exponential factor is denoted by A, T denotes the absolute temperature(K), the universal gas constant corresponds to R (J K $^{-1}$ mol $^{-1}$), h stands for Planck's constant, and N for the Avogadro number. The E_a^* values were computed via the slope value of the Arrhenius plot in Fig. 8, as appeared in Table 5. ΔH^* and ΔS^* were computed via plotting $\log(i/T)$ against 1/T (Fig. 8), as indicated in Table 5. It was found that the values of E_a^* are higher when the inhibitors are present than when they are not. When compared to the KB1 molecule, KB2 has a lower value of E_a^* , which indicates that its adsorption on the CS is chemical. However, the rise in the E_a^* could not be considered significant because of competitive adsorption with water, whose desorption from the surface also requires some activation energy, as documented in literature⁶⁸. The data gathered showed that the energy barrier for the dissolution reaction rises when inhibitors are present, and the dissolution becomes more difficult to happen with the existence of tested inhibitors, as implied by the positive

Fig. 9. Langmuir isotherms for the synthesized KB1 and KB2 utilizing data obtained *via* EIS and PP methods at 298 K.

	EIS			PP				
Compound	Slope	R^2	$K_{ads} x 10^4, M^{-1}$	- ΔG ^o _{ads} , kJ mol ⁻¹	Slope	R^2	$K_{ads} x 10^4, M^{-1}$	- ΔG° ads, kJ mol ⁻¹
KB1	1.11795	0.99984	24.9	40.7	1.07697	0.99154	12.1	38.9
KB2	1.07232	0.99869	85.8	43.8	1.07113	0.99999	50.8	42.5

Table 6. Langmuir isotherm parameters for KB1 and KB2 at 298 K.

values of ΔH^* , which suggests that the dissolution reaction is an endothermic process⁶⁹. The negative values of ΔS^* in the existence of KB1 and KB2 suggest that the activated complex favors association over dissociation, indicating the establishment of a stable inhibitor layer on the CS surface⁷⁰.

Adsorption process study

Studying adsorption isotherms is a potent tool for understanding the physicochemical interactions between corrosion inhibitors and metallic surfaces. Organic molecules inhibit corrosion by adsorbing onto the metal surface, displacing water molecules, and forming a protective barrier that blocks corrosive agents. In the H_2SO_4 solution, numerous models were studied to examine the connection regime at the inhibitors/CS interface and identify the best isotherm among the many adsorption isotherms^{52,71}. The Langmuir model (Eq. (7)) demonstrated optimal fitting, as confirmed by linear C/θ versus C plots (Fig. 9) with slopes and regression coefficients (R^2) approaching unity *via* EIS and PP approaches. This alignment validates the isotherm's applicability for adsorption analysis⁷².

$$\frac{C}{\theta} = \frac{1}{K_{ads}} + C, \tag{7}$$

where C represents the concentrations of KB1 and KB2, K_{ads} is the adsorptive equilibrium constant, and θ denotes the fractional surface covered by the employed inhibitors. K_{ads} can be computed from the intercept of Eq. (7). Equation (8) was utilized to obtain the standard free energy of adsorption ($\triangle G_{ads}^{\circ}$).

$$\Delta G_{ads}^{\circ} = -2.303 RT \log \left(K_{ads} x 55.5 \right), \tag{8}$$

where 55.55 designates the concentration of water in solution (M). The values of Langmuir isotherm parameters are provided in Table 6. The tested inhibitor molecules have a substantial adsorption ability as implied by the high K_{ads} values, resulting in improved corrosion resistance 73 . According to Table 6's data, ΔG_{ads}° values are negative, demonstrating that the inhibitors under study are adsorbing spontaneously on the CS surface. Based on literature 74 , ΔG_{ads}° values below -20 kJ mol $^{-1}$ suggest physisorption, which happens when the inhibitor and the surface interact electrostatically. On the other hand, values close to or higher than -40 kJ mol $^{-1}$ indicate chemisorption, which denotes the creation of coordination bonds through electron sharing or transfer. The adsorption of KB1 and KB2 onto the CS surface primarily happens via the chemisorption mechanism, which is started by physical interactions, according to the computed ΔG_{ads}° values.

Effect of immersion time

EIS is a practical method for evaluating the inhibition process after extended immersion 75 . The CS surface was subjected to 0.5 M $_2$ SO $_4$ solution at different immersion times, without and with 9×10^{-5} M of KB1 and KB2 at 298 K. The effects of KB1 and KB2 on CS corrosion in 0.5 M $_2$ SO $_4$ at various intervals are represented

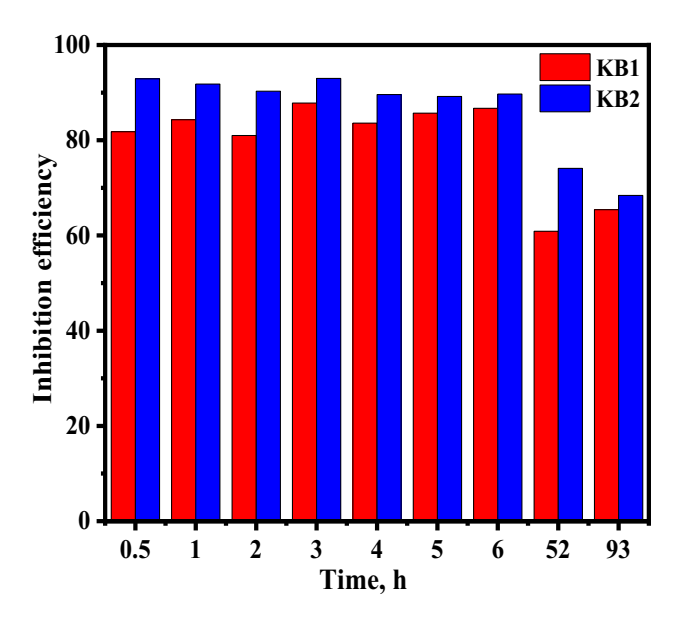


Fig. 10. The impact of lengthy immersion periods on the effectiveness of KB1 and KB2 inhibition for CS dissolution in 0.5 M $\rm H_2SO_4$ with $\rm 9\times10^{-5}$ M at 298 K.

Compound	Time, h	$R_{\rm s}$, Ω cm ²	$R_{\rm ct}$, Ω cm ² ± SD	Goodness of fit(x10 ⁻³)	θ	%IE
	0.5	2.124	69.44±1.69	5.528	-	-
	1	2.105	102.3 ± 1.44	5.424	-	-
	2	2.090	149.8 ± 2.08	5.673	-	-
	3	2.215	131.5 ± 2.16	4.560	-	-
Blank	4	2.109	229.0 ± 1.76	5.487	-	-
	5	2.120	262.0 ± 1.69	5.381	-	-
	6	2.125	286.0 ± 1.80	5.183	-	-
	52	2.137	699.4±1.31	4.691	-	-
	52 2.137 699.4±1.31 93 1.985 848.0±1.67 0.5 2.750 382.3±2.49 1 2.741 652.7±2.16 2 2.717 787.8±1.67 3 2.684 1075.0±1.59 4 2.653 1393.0±1.63	6.993	-	-		
	0.5	2.750	382.3 ± 2.49	3.217	0.818	81.8
	1	2.741	652.7 ± 2.16	3.597	0.843	84.3
	2	2.717	787.8 ± 1.67	3.310	0.810	81.0
	3	2.684	1075.0 ± 1.59	3.634	0.878	87.8
KB1	4	2.653	1393.0 ± 1.63	3.511	0.836	83.6
	5	2.630	1832.0 ± 2.74	3.813	0.857	85.7
	6	2.620	2150.0 ± 1.51	3.821	0.867	86.7
	52	2.641	1788.0 ± 1.68	3.043	0.609	60.9
	93	2.517	2453.0 ± 2.49	4.539		65.4
	0.5	2.970	977.9 ± 1.59	3.997	0.929	92.9
	1	2.923	1245.0 ± 1.51	4.592	0.918	91.8
	2	2.897	1540.0 ± 2.94	5.014	0.903	90.3
	3	2.936	1890.0 ± 1.63	4.984	0.930	93.0
KB2	4	2.936	2200.0 ± 1.45	5.152	0.896	89.6
	5	2.960	2420.0 ± 2.45	5.170	0.892	89.2
	6	2.945	2770.0 ± 2.49	5.269	0.897	89.7
	52	2.558	2700.0 ± 1.59	4.284	0.741	74.1
	93	2.568	2685.0 ± 1.40	4.463	0.684	68.4

Table 7. EIS parameters for CS in 0.5 M $\rm H_2SO_4$ without and with 9×10^{-5} M of KB1 and KB2 at various immersion times.

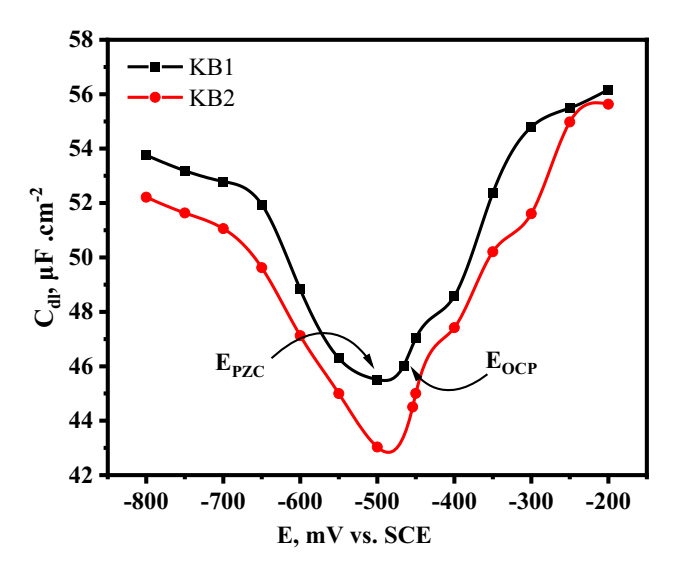


Fig. 11. The plot of C_{dl} vs. E for CS in 0.5 M H_2SO_4 solution with 5×10^{-5} M of KB1 and KB2 at 298 K.

Inhibitors	E _{ocp} (mV vs. SCE)	E _{PZC} (mV vs. SCE)	E _r (mV vs. SCE)
KB1	- 466	- 500	34
KB2	- 454	- 500	46

Table 8. Values of E_{ocp} , E_{PZC_5} and E_r recorded for CS in 0.5 M H_2SO_4 solution with 5×10^{-5} M of KB1 and KB2 at 298 K.

in Fig. 10. Table 7 provides the %IE values for different immersion times. The tested inhibitors demonstrated good stability and consistent inhibition performance, as indicated by the minimal change in %IE values over an extended immersion period of 6 h. All R_{ct} values were noticeably higher in the presence of KB1 and KB2 than in $\rm H_2SO_4$ solution-free, suggesting that the adsorbed layer shields the CS from the harsh effects of the acidic medium 66,76 . The disintegration of the inhibitor film may have caused a decrease in inhibitory action after 6 h. This investigation further demonstrates the high stability and effectiveness of the tested inhibitors.

Zero charge potential

The tested inhibitors are adsorbed from $\rm H_2SO_4$ solution onto the CS surface via chemical and physical interactions. The adsorption of inhibitors begins with physical interactions. After protonated molecules adsorb, charge sharing or transfer takes place between the metal's d orbitals and the molecules. Numerous factors, including the charge or dipole moment of the inhibitor molecules, the inhibitor's chemical structure, and the charge of the CS surface, can potentially influence the adsorption process⁷⁷. The PZC of the CS in the inhibited solution was defined via the EIS technique to obtain additional information regarding the surface charge of the CS. Figure 11 shows the dependence of double-layer capacitance ($\rm C_{dl}$) on the applied potential. The value of the CS's $\rm E_{PZC}$ corresponds to the minimum value of $\rm C_{dl}$. The surface charge is determined by the position of $\rm E_{ocp}$ relative to the $\rm E_{PZC}$ and Eq. (9) was used to calculate the net surface charge of the CS⁷⁸.

$$E_{\rm r} = E_{\rm ocp} - E_{\rm pzc} \tag{9}$$

where E_r stands for Antropov's "rational" corrosion potential. $E_r > 0$ denotes a positive net charge of the CS surface at open circuit potential, while $E_r < 0$ suggests a negative one. The CS surface was positively charged at the OCP when using KB1 and KB2, as implied by the positive E_r values for both inhibitors (Table 8). Due to electrostatic repulsion, protonated inhibitors find it challenging to approach the positively charged CS surface. On the other hand, adsorption of the SO_4^{2-} anion in aqueous H_2SO_4 solution is preferable since it generates an excess of negative charges. Nevertheless, because the SO_4^{2-} anion is more hydrated than Cl^- anion, it adsorbs poorly on the positively charged CS surface, leaving more active sites available for the inhibitors to adsorb directly onto the charged metal surface. Also, it is crucial to remember that protonated species of KB1 and KB2 may be discharged on the CS surface, so neutral molecules that result may be able to adsorb on the surface of CS following chemisorption mechanisms *via* the unshared pair of electrons on the heteroatoms (N and S) to reduce metal disintegration by providing a protective chemisorbed layer⁵².

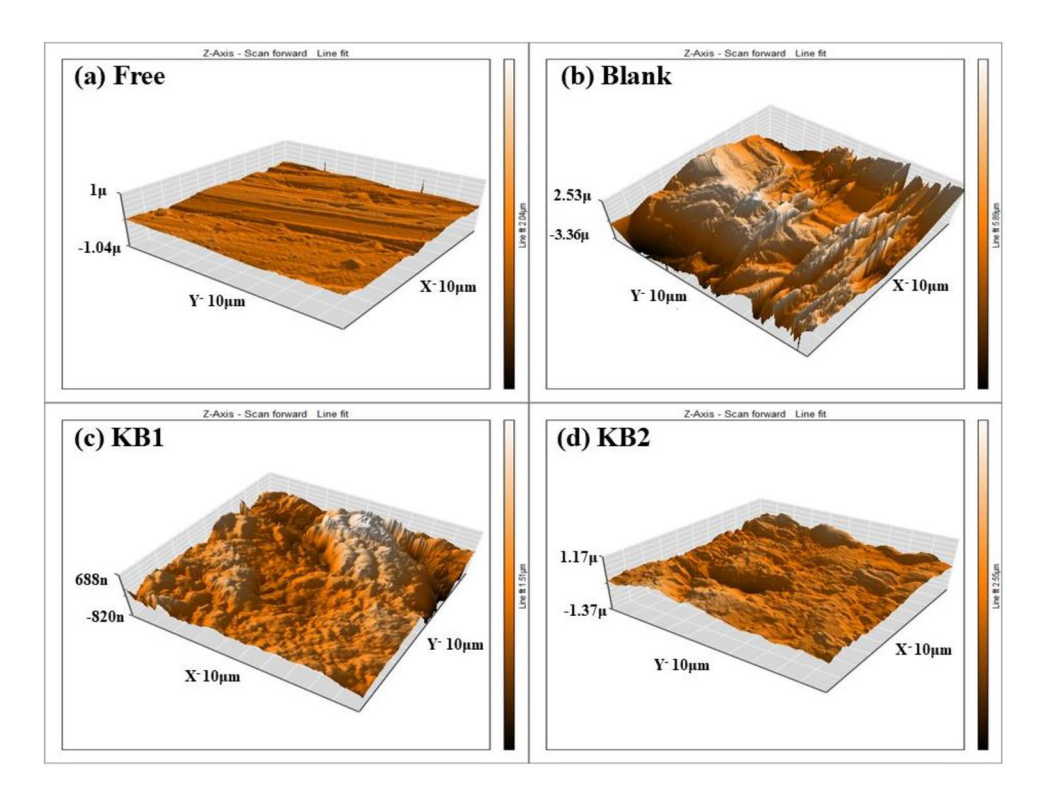


Fig. 12. 3D AFM images of the surface of polished CS (**a**), following immersion in 0.5 M H₂SO₄ solution before (**b**) and after the addition of KB1(**c**), and KB2 (**d**) for one day at 298 K.

Surface characterization

AFM analysis

Metal surface roughness can be evaluated using AFM analysis 79 . To test the compounds' ability to impede corrosion, the CS coupons were submerged in the blank solution for 24 h at 298 K without and with 9×10^{-5} M of KB1 and KB2. Figure 12a–d depicts three-dimensional AFM images of the CS surfaces. Before the CS immersion in 0.5 M $_2$ SO₄, the CS's surface appeared smooth with a roughness value of 34.16 nm (Fig. 12a), following immersion in 0.5 M $_2$ SO₄ (Fig. 12b), the surface was damaged and became rougher and the roughness value increased to 853.81 nm, adding KB1 and KB2 made the surface smoother and the roughness values diminished to 153.88 nm and 114.65 nm, respectively when related to the blank sample (Fig. 12c and d). The lower roughness value for KB2 indicates that it protects the CS more effectively than KB1 in 0.5 M $_2$ SO₄ by adhering to the CS surface and forming a protective film $_2$ SO₄ by adhering to the CS surface and forming a protective film $_2$ SO₄ by adhering to the CS surface and forming a protective film $_2$ SO₄ by adhering to the CS surface and forming a protective film $_2$ SO₄ by adhering to the CS surface and forming a protective film $_2$ SO₄ by adhering to the CS surface and forming a protective film $_2$ SO₄ by adhering to the CS surface and forming a protective film $_2$ SO₄ by adhering to the CS surface and forming a protective film $_2$ SO₄ by adhering to the CS surface and forming a protective film $_2$ SO₄ by adhering to the CS surface and forming a protective film $_2$ SO₄ by adhering to the CS surface and forming a protective film $_2$ SO₄ by adhering to the CS surface and forming a protective film $_2$ SO₄ by adhering to the CS surface and forming a protective film $_2$ SO₄ by adhering to the CS surface and forming a protective film $_2$ SO₄ by adhering to the CS surface and forming a protective film $_2$ SO₄ by adhering to the CS surface and forming a protective film $_2$ SO₄ by adhering to the CS surface and forming the CS surface and fo

XPS analysis

The surface phenomena were examined using XPS to fully comprehend the elements of the adsorbed layer that developed on the exposed portion of CS submerged in 0.5 M H_3SO_4 solution with 9×10^{-5} M of KB1 and KB2 after immersion for 24 h, as indicated in the acquired XPS spectra in Figs. 13 and 1482. The binding energies (BE, eV) with the assignment for each peak component are indicated in Table 9. As depicted in Figs. 13 and 14, the spectra comprise C 1s, N 1s, O 1s, Fe 2p, and S 2p, supporting the adsorption of KB1 and KB2 on the CS surface. Three peaks were visible in the C1s XPS spectra for KB1 and KB2. The C-H, C-C, and C=C bonds may cause the first peak, which is located at 284.88 and 285.08 eV⁸³. The C-N bonds may be connected to the second peak, which is located at 286.28 and 286.68 eV, while the last peaks, at 288.38 and 288.58 eV, may be associated with C=N bonds, which are included in the structures of KB1 and KB2 and confirm their adsorption⁸⁴. The XPS spectra of O 1s exhibited three peaks (Figs. 13 and 14). The first and second peaks, observed at 530.18 and 531.68 eV respectively, correspond to $\mathrm{Fe_2O_3}$ / $\mathrm{Fe_3O_4}$ and FeOOH. The third peak, at 532.58 and 532.78 eV, is associated with adsorbed water molecules 85. XPS spectra of Fe 2p exhibit seven distinct peaks (Figs. 13 and 14). Metallic iron is characterized by peaks at 707.29 eV and 711.24 eV. The Fe³⁺ state is identified at 710.88 and 711.18 eV, while Fe³⁺ is at 712.88 and 713.98 eV. The 716.28 and 716.98 eV peaks may be related to Fe 2p_{3/2} of Fe²⁺. Additionally, satellite peaks of Fe³⁺ are observed at 719.88 and 720.18 eV. The Fe $2p_{1/2}$ component of Fe²⁺ appears at 724.48 eV, whereas Fe $2p_{1/2}$ of Fe³⁺ exhibits peaks at 726.98 and 727.18 eV. Finally, the Fe $2p_{1/2}$ component of Fe²⁺ is detected at 730.18, 729.98, 733.58, and 733.18 eV⁵⁸. Nitrogen's XPS spectra (Figs. 13 and 14) showed two peaks, the first at 399.18, 398.78 eV, and the second at 400.88, 400.78 eV, which stand for N-H/ N-H₂, N-Fe, N- \bar{N}^{86} and C=N-N bonds⁸⁷ respectively. Four peaks for S2p appeared in the XPS spectra (Figs. 13 and 14). The first at 161.58, 162.58, and 163.88 eV stand for sulphide and S-C bonds, while the second at 166.78, 166.68, 168.48, and 170.08 eV ascribed to S-Fe bonds⁸⁷. Based on the XPS data, the adsorption of KB1 and KB2 on CS was proved.

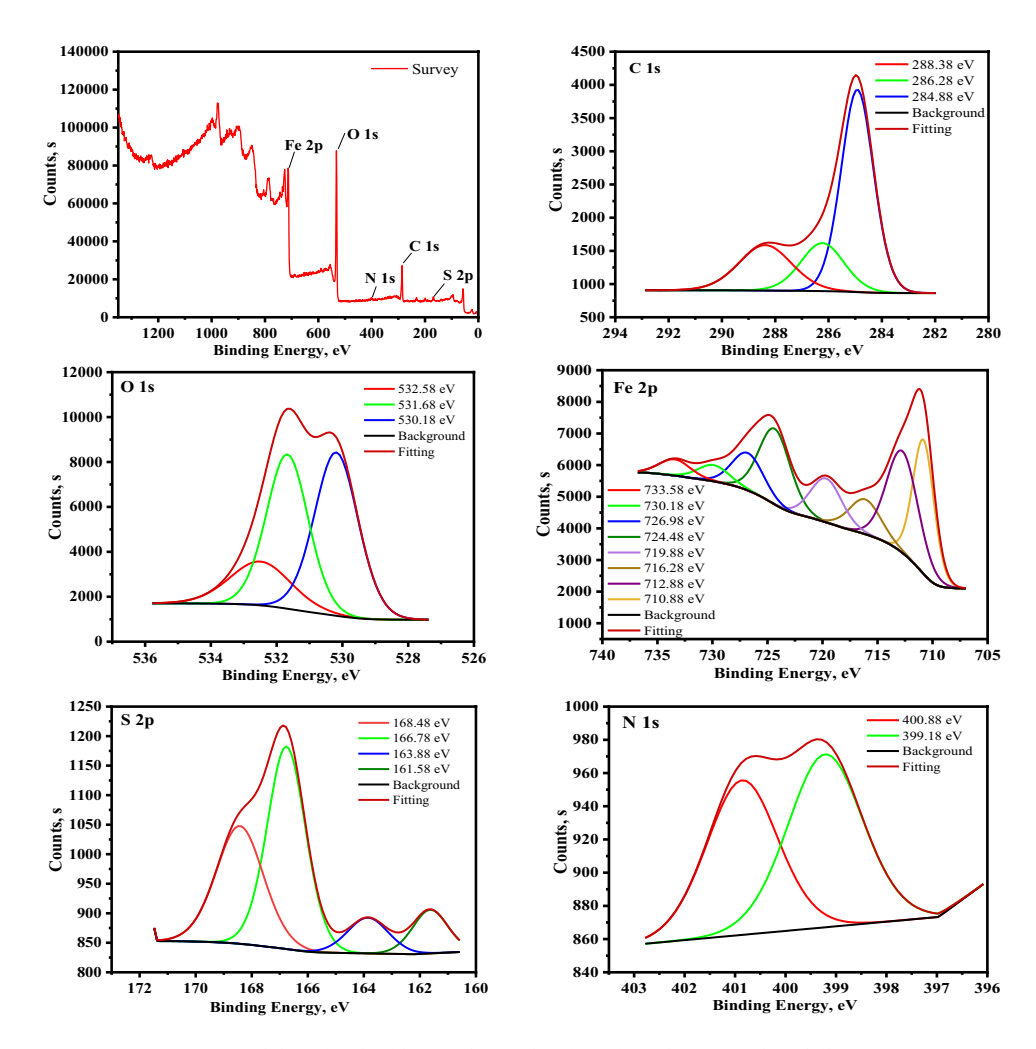


Fig. 13. XPS spectra of the adsorbed layer of KB1 developed on the CS surface following immersion in 0.5 M $\rm H_2SO_4$.

Core element	0.5 M H ₂ SO ₄ +	KB1	0.5 M H ₂ SO ₄ +KB2		
	BE, eV	Assignments	BE, eV	Assignments	
	284.88	C-H, C-C, and C=C	285.08	C-H, C-C, and C=C	
C 1s	286.28	C-N	286.68	C-N	
	288.38	C=N	288.58	C=N	
	530.18	Fe ₂ O ₃ / Fe ₃ O ₄ oxide	530.18	Fe ₂ O ₃ and/or Fe ₃ O ₄ oxide	
O 1s	531.68	FeOOH	531.68	FeOOH	
	532.58	Adsorbed water molecules	532.78	Adsorbed water molecules	
	710.88	Metallic iron	711.18	Metallic iron	
	712.88	Fe ³⁺	713.98	Fe ³⁺	
	716.28	Fe 2p _{3/2} of Fe ²⁺	716.98	Fe 2p _{3/2} of Fe ²⁺	
Fe 2p	719.88	Satellite of Fe ³⁺	720.18	Satellite of Fe ³⁺	
	724.48	Fe 2p _{1/2} of Fe ²⁺	724.48	Fe 2p _{1/2} of Fe ²⁺	
	726.98	Fe 2p _{1/2} of Fe ³⁺	727.18	Fe 2p _{1/2} of Fe ³⁺	
	730.18, 733.58	Fe 2p _{1/2} of Fe ²⁺	729.98, 733.18	Fe 2p _{1/2} of Fe ²⁺	
N 1s	399.18	N-H/N-H ₂ , N-Fe, N-N	398.78	N-H/N-H ₂ , N-Fe, N-N	
N 18	400.88	C=N-N	400.78	C=N-N bond	
C 2m	161.58,163.88	Sulphide, S-C	162.58	Sulphide, S-C	
S 2p	166.78,168.48	S-Fe	166.68,168.48,170.08	S-Fe	

Table 9. The binding energies (eV) with their assignments for the CS after being immersed in 0.5 M $\rm H_2SO_4$ containing 9×10^{-5} M of KB1 and KB2.

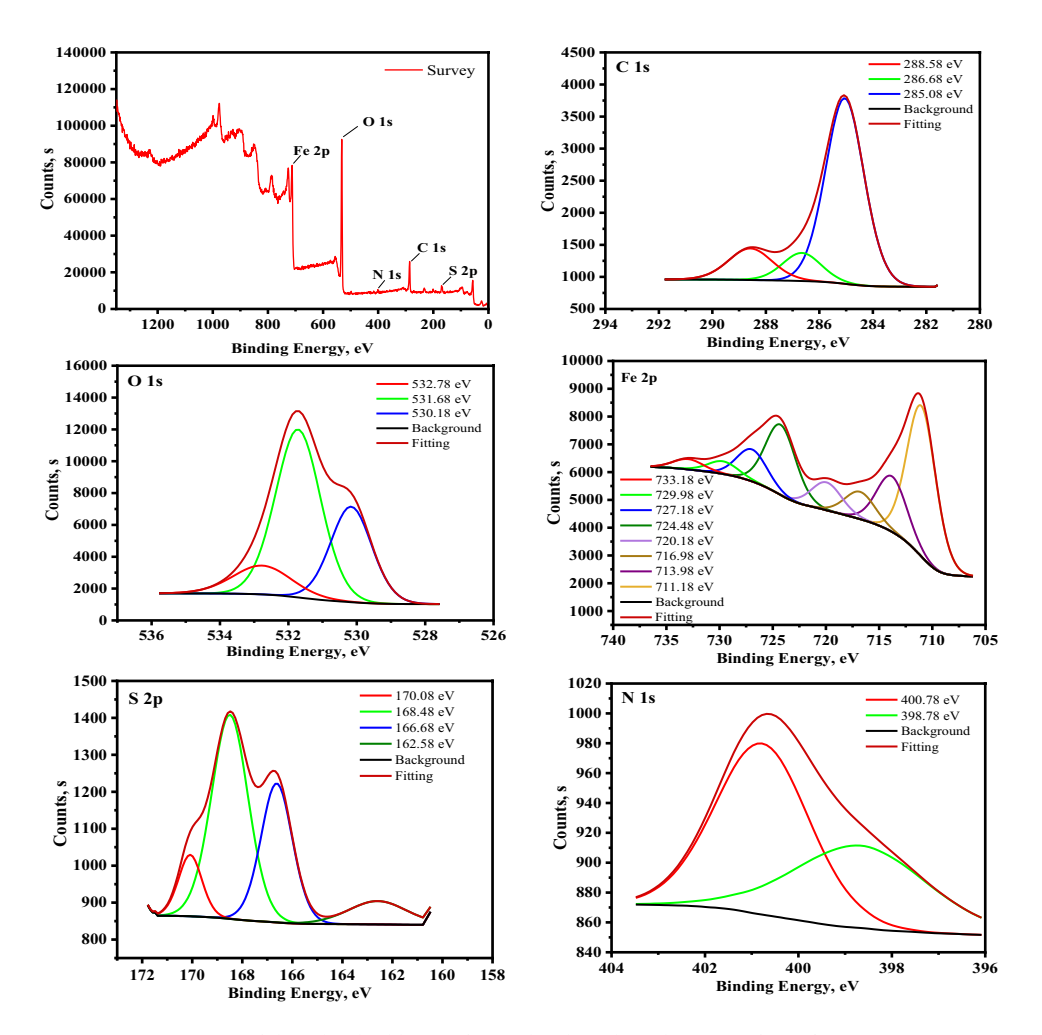


Fig. 14. XPS spectra of the adsorbed layer of KB2 developed on the CS surface after immersion in 0.5 M $_{\rm H_2SO_4}$.

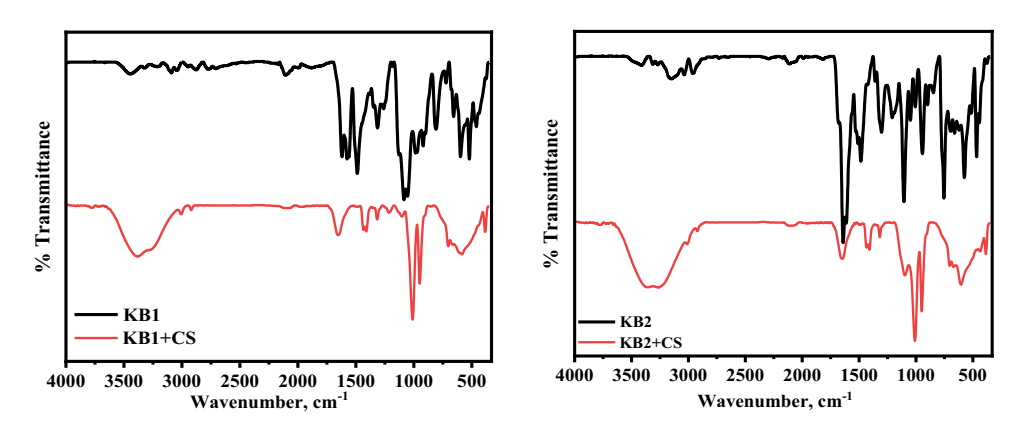


Fig. 15. FT-IR spectra of the pure inhibitor and the layers that developed on CS samples after one day of immersion in $0.5 \text{ M H}_2\text{SO}_4$ with $9 \times 10^{-5} \text{ M}$ of inhibitors at 298 K.

FT-IR analysis

Figure 15 presents the utilization of infrared spectroscopy to confirm the interaction among the inhibitors and the CS surface in 0.5 M H₂SO₄. The comparison of spectra for pure inhibitors and the layers that developed on CS samples show that the inhibited CS coupons resemble that of the free inhibitors, with shifts observed in the spectra, likely due to the interaction among inhibitor molecules and the CS surface, offering definitive evidence of inhibitor adsorption on the metal surface, thereby facilitating corrosion protection⁸⁸. The shifting

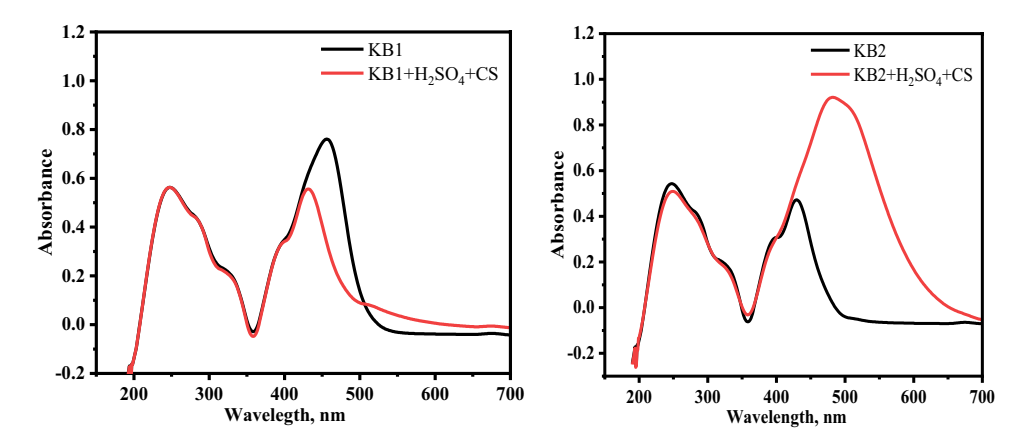


Fig. 16. UV-visible spectra for test solutions of KB1 and KB2 before (black color) and after (red color) dipping CS for 48 h at 298 K.

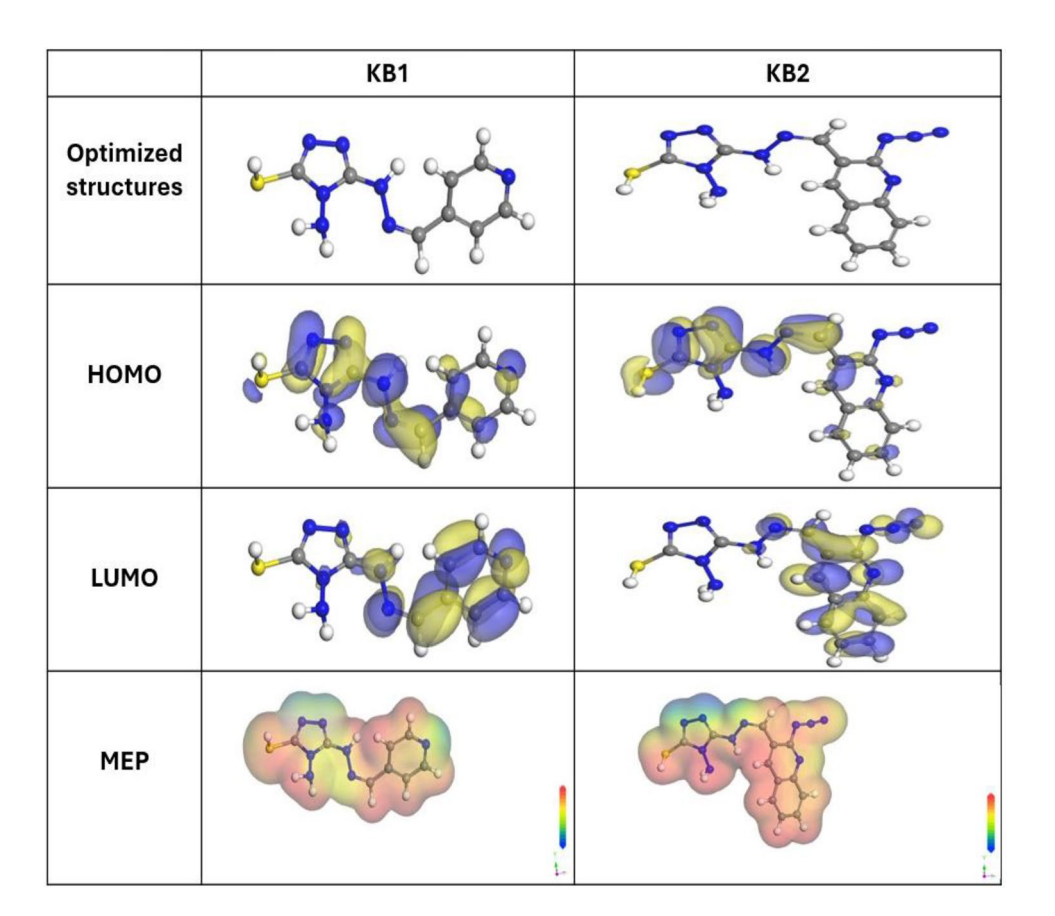


Fig. 17. The optimized structures, HOMO, LUMO, and MEP of the KB1 and KB2 using DMol³ module.

and removal of some peaks in the spectra after immersion indicated that the inhibitors effectively adsorbed onto the surface of CS *via* functional groups, resulting in inhibition ^{89,90}.

UV-Visible spectra

To verify the potential for developing the inhibitor-Fe complex, Fig. 16 displays the UV-Visible absorption spectra recorded for the test solutions of 9×10^{-5} M of KB1 and KB2 before and after 48 h of CS immersion at 298 K. Before CS immersion, absorption bands for KB1 and KB2 are visible in the spectra at (248 nm, 456 nm) and (247 nm, 429 nm), respectively, which are ascribed to π - π *and n- π * possessing a significant charge transfer characteristic^{91,92}. However, after CS immersion, the spectra exhibited changes in the location of absorption bands. The KB1 spectrum displayed two distinct bands at 247 nm and 431 nm, while the observed bands for KB2 appeared at 249 nm and 482 nm. The alteration in the absorption maximum (λ_{max}) and/or the shift in

Quantum parameters	KB1	KB2
E _{HOMO} , eV	- 5.11	- 4.98
E _{LUMO} , eV	- 2.26	- 2.48
$\Delta E = E_{LUMO} - E_{HOMO}$, eV	2.85	2.50
I, eV	5.11	4.98
A, eV	2.26	2.48
χ, eV	3.68	3.73
η, eV	1.42	1.25
σ, eV	0.70	0.80
ΔN, eV	1.16	1.31
ΔE _{back-donation} , eV	- 0.36	- 0.31
Dipole moment value, debye	6.93	13.29
Molecular surface area, Ao2	252.02	329.54

Table 10. Quantum chemical parameters for KB1 and KB2.

absorbance values indicate the development of a complex between the tested inhibitor molecules and the Fe^{2+} ions in solution, as reported in literature⁹³. These experimental results provide strong evidence for the formation of a protective metal/inhibitor complex film on the CS, confirming the complexation between Fe^{2+} and KB1/KB2 in H_2SO_4 solution⁹⁴.

Theoretical calculations

DFT

Figure 17 presents the optimized structures alongside the spatial distributions of the highest occupied molecular orbital (HOMO), the lowest unoccupied molecular orbital (LUMO), and molecular electrostatic potential (MEP) mapping for the KB1 and KB2 molecules in an aqueous environment. The corresponding theoretical parameters are provided in Table 10. Based on Frontier Molecular Orbital (FMO) theory, the interaction between a molecule and a metallic surface can be elucidated through the analysis of HOMO and LUMO energy levels, which offer valuable insight into the molecule's electron-donating and -accepting capabilities. These energy levels determine whether a molecule exhibits anticorrosive properties95. Higher HOMO energy and lower LUMO energy generally correlate with enhanced anticorrosive performance. KB2 molecules exhibit a higher E_{HOMO} (- 4.98 eV) than KB1 molecules (- 5.11 eV), according to the findings in Table 10, indicating that KB2 possesses superior corrosion inhibition capabilities. It is evident from Fig. 17 that the HOMO orbital for KB1 and KB2 concentrated on the triazole, hydrazone, pyridine, and quinoline moieties, rendering these areas more vulnerable to electrophilic assaults on the CS. The findings of the experiments support the idea that the tested inhibitor molecules can efficiently adhere to the CS, strengthening their protective impact against corrosion. Compared to the KB1 molecules, which have an E_{LUMO} value of -2.26 eV, the KB2 molecules exhibit a lower E_{LUMO} (- 2.48 eV), suggesting that KB2 has a greater propensity for adsorption than KB1. Because it is desirable for enabling the transport of an electron from the inhibitor to the metallic surface, reducing the energy gap (ΔE) is essential for increasing the effectiveness of corrosion inhibitors ⁹⁶. In Table 10, KB2 has ΔE of 2.50 eV, significantly lower than the ΔE of KB1 (2.85 eV), demonstrating the increased susceptibility for the adsorption of KB2 onto CS. Corrosion inhibitors often possess low electronegativity (χ) values, reflecting their ability to donate electrons to the metal, thereby enhancing their protective performance⁹⁷. However, the inhibitor molecule can receive the electron from the metal surface if its χ value is high. It occurs through backdonation, which enhances the bond at the steel interface 98. The molecules of KB1 and KB2 have relatively high χ values, which facilitate the back-donation of electrons and promote the formation of more stable interactions with the CS, as detailed in Table 10. Furthermore, the reactivity and stability of inhibitor molecules can be evaluated through their global softness (σ) and hardness (η) parameters. The smooth passage of electrons to the CS via adsorption gives the soft molecules greater protective capacity than the hard molecules, rendering them effective corrosion inhibitors⁹⁹. Table 10 illustrates that the KB2 molecule has better inhibitory properties than the KB1 molecule because of its greater σ and lower η values. Additionally, the number of electrons transferred (ΔN) and $\Delta E_{back-donation}$ are pivotal factors in assessing the inhibitor's capacity to give or accept electrons. It is suggested that electron transfer from the inhibitor to the metal occurs if ΔN values are higher than 0. Conversely, electron transfer from the metal to the inhibitor molecule is feasible if ΔN values (< 0)¹⁰⁰. The molecules of KB1 and KB2 have positive ΔN values, which indicate their ability to supply electrons to the CS, as recorded in Table 10. Moreover, the $\Delta E_{back-donation}$ becomes less than zero when $\eta > 0$, indicating that electrons are moved from the metal to the inhibitor and then donated back to the metal. This dynamic process is desirable 101. Table 10 presents negative $\Delta E_{back-donation}$ values for KB1 and KB2, suggesting their strong tendency for back-donation and the development of robust bonds⁴⁷. The dipole moment (μ) indicates how polarizable the tested inhibitors are. A high value of μ suggests strong polarizability, which in turn shows high reactivity, prompting inhibitors to adhere to the surface firmly ¹⁰². As mentioned in Table 10, KB2 has a higher dipole moment value (13.29 Debye) than KB1 (6.93 Debye), emphasizing its higher tendency to be adsorbed onto the CS, as well as strengthening its inhibitory impact. A noticeable correlation was observed among the molecular surface area of the tested inhibitors and their ability to safeguard the CS from dissolution. A larger molecular surface area enhances the inhibition efficiency and increases the contact area on the CS¹⁰³. As presented in Table 10, KB2 exhibited a larger

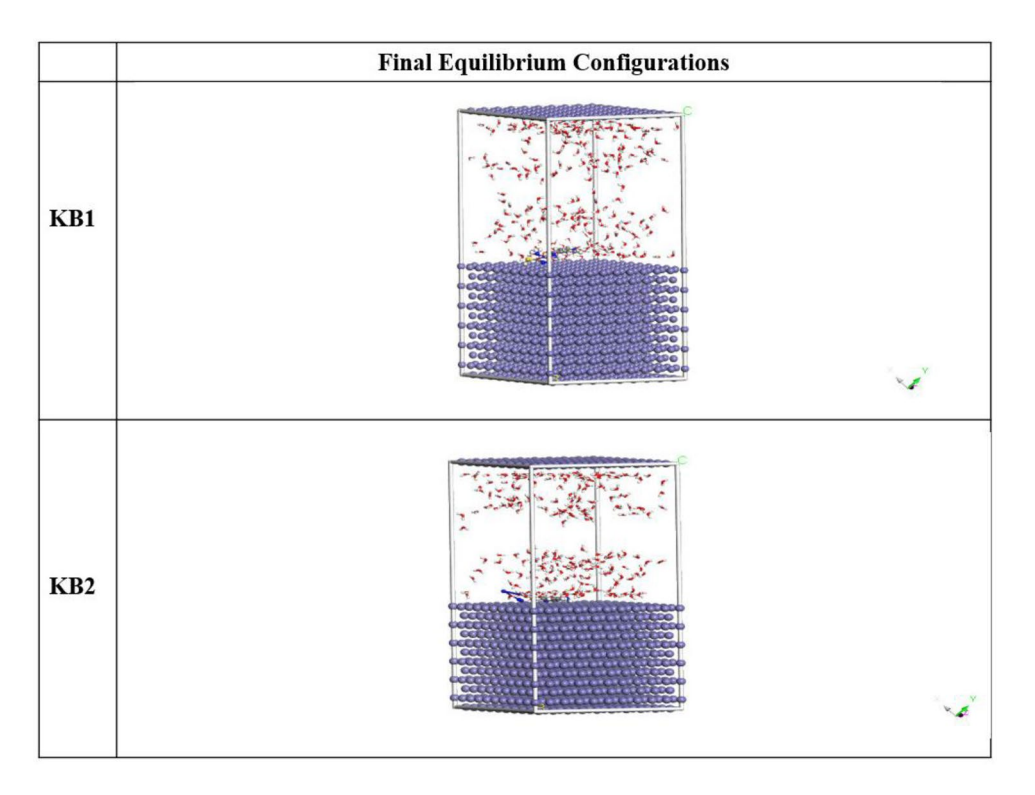


Fig. 18. The most suitable configuration for the adsorption of KB1 and KB2 on Fe (110).

Structures	Adsorption energy/kcal mol ⁻¹	Rigid adsorption energy/ kcal mol ⁻¹	Deformation energy/kcal mol ⁻¹	$\frac{dE_{ads}/dN_i: inhibitor, kcal}{mol^{-1}}$	dE _{ads} / dN _i : water, kcal mol ⁻¹
Fe (1 1 0) KB1 Water	- 3030.47	- 3181.06	150.59	- 142.41	- 7.75
Fe (1 1 0) KB2 Water	- 3083.62	- 3240.13	156.51	- 172.48	- 7.54

Table 11. The MC simulation data for the adsorption of the KB1 and KB2 on Fe (110).

molecular surface area (329.54 Ų), resulting in greater inhibition efficiency when compared to KB1(252.02 Ų). The inhibitors' active sites may be investigated *via* MEP mapping, a three-dimensional visual depiction that uses a molecule's general charge distribution to determine its net electrostatic effect¹⁰⁴. The red areas in Fig. 17 indicate the highest electron density, where the MEP is highly negative (nucleophilic reaction). In the meantime, the blue areas indicate the highly positive areas (electrophilic reaction)¹⁰³. The highly negative regions in Fig. 17 are centered over free nitrogen, sulphur, pyridine, and quinoline moieties. In contrast, the highly positive areas over the triazole ring's allocated nitrogenous atoms are due to the hybridization of lone pairs allocated on the nitrogenous atoms at positions (1,2) is the sp² orbital, which is allocated in the same plane of the ring and does not overlap with other p orbitals of the ring. The areas with higher electron densities (shown by the red area) for KB1 and KB2 molecules are probably the most desirable for interactions with the CS, resulting in the configuration of sustainable protective layers.

MC simulation

The best adsorption configurations and interactions between the tested inhibitors and the CS surface were investigated *via* MC simulations¹⁰⁵. The most desirable adsorption configurations of KB1/KB2 are displayed in Fig. 18. KB1 and KB2 molecules are nearly parallel to the Fe (110) surface as a result, CS in the corrosive solution can be kept from corroding as much as possible *via* parallel adsorption which optimizes the surface-coverage characteristics of the inhibitors¹⁰⁶. The adsorption energies computed *via* MC in Table 11 demonstrate significantly stronger adsorption for KB2, evidenced by its more negative adsorption energy (– 3083.62 kcal/mol) compared to KB1 (– 3030.47 kcal/mol). These results support the idea that KB2 could form a firmer adsorptive layer on the CS, enhancing corrosion resistance¹⁰⁷. Furthermore, Table 11 asserts a higher inhibition proficiency for KB2 than KB1 by demonstrating that the adsorption energies values of KB2 for the pre-geometry

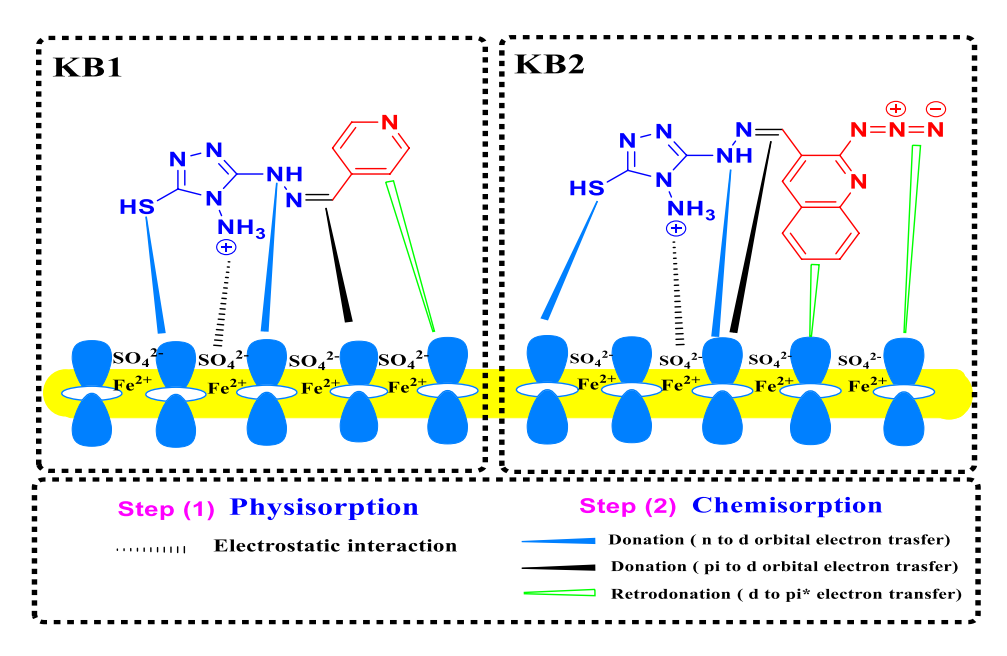


Fig. 19. A schematic representation of the corrosion inhibition mechanism for CS in 0.5 M H₂SO₄.

optimization step, or unrelaxed ($-3240.13~kcal~mol^{-1}$), are more negative than KB1 ($-3181.06~kcal~mol^{-1}$) and for the post-geometry optimization step, or relaxed ($156.51~kcal~mol^{-1}$), respectively), are higher than KB1 ($150.59~kcal~mol^{-1}$). If water molecules or adsorbed inhibitors have been removed, the dE ads/dN_i values provide insight into the metal-adsorbates configuration energy 108 . In Table 11, the dE ads/dN_i value for KB2 is much higher ($-172.48~kcal~mol^{-1}$) than the KB1 molecule ($-142.41~kcal~mol^{-1}$). Accordingly, the KB2 molecule has a higher propensity for adsorption than the KB1 molecule. Furthermore, the dE ads/dN_i values for water are low (about $-7.65~kcal~mol^{-1}$) when compared to KB1 and KB2 values, indicating that inhibitor molecules adsorbed more robustly than water molecules, reinforcing the replacement of water molecules *via* tested inhibitor molecules 109 . Due to this replacement, a coherent protective layer developed onto the CS in the corroding medium. These computational findings are consistent with the observed experimental data on corrosion resistance.

Corrosion Inhibition mechanism

Considering the theoretical and experimental results, Fig. 19 depicts the possible mechanism of corrosion inhibition for CS in $0.5 \, \mathrm{M} \, \mathrm{H}_2 \mathrm{SO}_4$. According to the literature 110 , the adsorption between the inhibitor and the CS surface can occur physically, chemically, or both. Physical, which results from electrostatic interactions between the charged CS surface and the protonated groups of organic molecules 111 . In this context, the protonated inhibitors in $\mathrm{H}_2\mathrm{SO}_4$ can be adsorbed on CS surfaces through interaction with the negatively charged surface (caused by the adsorbed SO_4^{2-} ions on it), resulting in physical adsorption. On the other hand, there are two strategies to achieve the chemical adsorption of the tested inhibitors on the CS surface through donor-acceptor interaction 90 . The first involves the interaction of π -electrons on the nitrogen atoms and π -electrons of the aromatic moieties and the vacant d-orbital of the CS, inhibiting it from dissolving in the corrosive medium. The second is accomplished by the formation of the Fe-inhibitor complex, which results from the chemical coordination of iron atoms as electron acceptors and the inhibitor's heteroatoms as electron donors. Retrodonation, in which orbital electrons are transferred from the metal atoms to the inhibitor molecules' antibonding molecular orbitals, is another way that inhibitor molecules might attach to metal surfaces 112 . The %IE of these derivatives is in the order KB2 > KB1, which is explained by the presence of quinoline moiety and azido group in the structure of KB2. Also, it has a lower energy gap and a higher softness value, which increases the availability of donation and retro-donation, thus improving and strengthening its adsorption on the CS surface.

Comparative studies with previous reports

Notably, our compounds exhibited high inhibition efficiencies even at relatively low concentrations, whereas many literature-reported inhibitors required significantly higher concentrations to achieve comparable efficiency values, as indicated in Table 12. This demonstrates both the cost-effectiveness of KB1 and KB2 as well as their improved corrosion inhibition capabilities, as lower amounts are needed to protect the surface of CS. We think that this comparison gives an improved overview of the economic and practical benefits of our eco-friendly inhibitors.

Conclusion

1. In this study, we synthesized and characterized two triazole compounds, KB1 and KB2. These compounds were then tested for their ability to impede dissolution in 0.5 M H₂SO₄ via different electrochemical technical

		Conc. of	% IE			
Inhibitor	Corrosive medium	inhibitor (mol/L)	PP	EIS	Sample	Reference
4-Amino-1-((8-hydroxyquinolin-5-yl)methyl)-1,2,3-triazole-5-carboxylate (MHTC)	1.0 M HCl	10 -3	91	87	carbon steel	113
5-((Furan-2-yl)methyleneamino)-2 <i>H</i> -1,2,4-triazole-3-thiol (FMT)	1.0 M HCl	5.0×10^{-3}	86	90	Mild stool	114
5-((Thiophen-2-yl)methyleneamino)-2 <i>H</i> -1,2,4-triazole-3-thiol (TMT)	1.0 WI HCI	3.0 × 10	90	93	carbon steel Mild Steel Mild Steel Carbon steel Mild Steel Mild Steel Mild Steel Carbon steel Mild Steel Mild Steel Mild Steel Mild Steel Carbon steel Carbon steel Carbon steel	
4-Amino-1,2,4- triazole-3-thiol (ATT)			98.56	94.82		
4-Amino-5-methyl-1,2,4-triazole-3-thiol (AMTT)	1.0 M H ₂ SO ₄	1.0×10^{-3}	99.39	95.72	Mild Steel	115
4-Amino-5-ethyl-1,2,4- triazole-3-thiol (AETT)			99.55	95.89	carbon	
Ethyl4-amino-1-((8-hydroxyquinolin-5-yl)methyl)-1 <i>H</i> -1,2,3-triazole-5-carboxylate (EHTC)			95.5	94.1		
4-Amino-1-((8-hydroxyquinolin-5-yl)methyl)- 1H-1,2,3-triazole-5-carbonitrile (AHTC)	0.5 M H ₂ SO ₄	10^{-3}	95.1	93.6		116
Methyl 4-amino-1-((8-hydroxyquinolin-5-yl)methyl)-1 <i>H</i> -1,2,3-triazole-5- carboxylate (MHTC)			94.1	93.9		
5-Octylsulfanyl-1,2,4-triazole (TR8)	1.0 M HCl	10-3	84.41	88.02	carbon steel Mild steel 2 Mild Steel 3 Carbon steel Mild Steel 4 Mild Steel 2 Carbon steel Mild Steel 4 Mild Steel 4 Mild Steel 6 Carbon steel 7 Mild Steel 8 Carbon steel 9 Carbon steel	117
5-Decylsulfanyl-1,2,4-triazole (TR10)	1.0 WITICI	10	85.60	92.00		
4-Amino-3-(N-phthallimidomethyl)-1,2,4-triazole-5- thione (Tz-1)	1.0 M HCl	2.5×10^{-4}	95.36	95.16	Mild ataal	118
3-(N-Phthalimidomethyl)-4-(4-pyridine)amino-1,2,4-triazole-5-thione (Tz-2)	1.0 M HCI	2.5 × 10	92.45	93.82	Willa steel	
1-((1H-1,2,4-triazol-3-ylimino)methyl) naphthalen-2-ol (TMN)			88.87	91.12		
N-(Furan-2-ylmethylene)-1 <i>H</i> -1,2,4-triazol-3-amine (FTA)	1.0 M HCl	10×10^{-4}	80.46	84.65		119
N-(Thio phen-2-ylmethylene)-1 <i>H</i> -1,2,4-triazol-3-amine (TTA)			80.51	86.19		
4-Amino-5-phenyl-4H-1, 2, 4,- triazole-3-thiol (APTT)			94.32	96.04		
4-Amino-5-(2-hydroxy) phenyl-4 <i>H</i> -1, 2, 4,-triazole-3-thiol(AHPTT)	1.0 M HCl	5.72×10^{-4}	93.05	95.40	Mild Steel	120
4-Amino-5-styryl-4H-1, 2, 4,-triazole-3-thiol, (ASTT)	1		96.45	97.03	1	
(Z)-4-Amino-5-(2-(pyridin-4-ylmethylene)hydrazinyl)-4H-1,2,4-triazole-3-thiol (KB1)	O.F.M.H.CO	9×10 ⁻⁵	87.50	86.90	CS	Our work
(Z)-4-Amino-5-(2-((2-azidoquinolin-3-yl)methylene)hydrazinyl)-4H-1,2,4-triazole-3-thiol (KB2)	0.5 M H ₂ SO ₄	9 × 10 -	91.40	92.40	CS	Our Work

Table 12. Comparison of studied inhibitors with some reported Triazole derivatives.

niques (OCP, PP, and EIS), surface characterizations, UV-Visible spectroscopy, and theoretical investigations

- 2. The results showed that both KB1 and KB2 inhibitors effectively impeded the corrosion of CS in the acidic medium, with KB2 exhibiting the highest protection efficiency of 92.4% at a dose of 9×10^{-5} M.
- 3. The tested compounds were identified as mixed-type inhibitors *via* the PP measurement.
- 4. The addition of KB1 and KB2 results in a decrease in double-layer capacitances relative to the blank solution. This validates their adsorption on the CS.
- 5. Analysis of the inhibitors' adsorption behavior revealed that they aligned with the Langmuir adsorption isotherm. According to thermal studies (298–328 K), strong adsorptive interactions with the CS are indicated by the inhibitors' improved inhibition at 318 K (88.9% for KB1 and 93.6% for KB2), then decreased at 328 K, which implies that higher temperatures (328 K) may cause the desorption of KB1 and KB2 from the CS.
- 6. The slight change in %IE value during a long immersion period extended to 6 h implies the stability of the protective film developed by KB1 and KB2 onto the CS. To investigate the inhibitory mechanism, ZCP measurements were employed, which demonstrate that the inhibitors first engaged in electrostatic interaction with the positively charged CS surface. After this, robust chemical bonds are formed.
- 7. Surface characterization techniques (AFM, XPS, and FT-IR) verified that the CS surface had a protective film that successfully protected it from the H₂SO₄ environment. The potential for complex establishment between ferrous ions and the tested inhibitors was validated *via* UV-visible spectroscopy.
- 8. DFT and MC simulations have explored the molecular structure, reactivity, and adsorption configuration of KB1 and KB2. They validated the placement of their multi-active sites and supported the experimental findings. The data acquired in this report highlights the potential application of synthesized triazoles as potent inhibitors against dissolution in metal treatment processes.

Data availability

All data generated or analysed during this study are included in this published article (and its Supplementary Information files).

Received: 10 May 2025; Accepted: 4 July 2025

Published online: 24 July 2025

References

- Singh, A. et al. Heteroatomic organic compound as a novel corrosion inhibitor for carbon steel in sulfuric acid: detail experimental, surface, molecular Docking and computational studies. Colloids Surf. Physicochem Eng. Asp. 673, 131692 (2023).
- Hakimi, H., Karimi, S. & Rezaeivala, M. Comparative study of morpholine-based ligands on corrosion Inhibition of C-steel in 0.5 M H₂SO₄ solution: chemical and electrochemical exploration. *Thin Solid Films*. 800, 140390 (2024).

- Abbout, S. et al. Gravimetric, electrochemical and theoretical study, and surface analysis of novel epoxy resin as corrosion inhibitor of carbon steel in 0.5 M H₂SO₄ solution. J. Mol. Struct. 1245, 131014 (2021).
- 4. EL-Zekred, M. A., Fouda, A., Nofal, A. M. & Shalabi, K. *Plantago major* extract as an environmentally friendly inhibitor for the corrosion of L-80 carbon steel in 0.5 M H₂SO₄ media. *Biointerface Res. Appl. Chem.* 11, 12186–12201 (2021).
- 5. Mohsen, O. A. et al. Indole derivatives efficacy and kinetics for inhibiting carbon steel corrosion in sulfuric acid media. *Results Eng.* 23, 102755 (2024).
- 6. Fang, Z. et al. Developing a novel Imine derivative as a corrosion inhibitor for Q235 carbon steel in 1 M HCl solution: experiments and theoretical calculations. *Mater. Today Commun.* **40**, 109693 (2024).
- 7. Modwi, M. M. Y. et al. Eco-friendly corrosion inhibitor of Q235 carbon steel in 1.0 M HCl by isatin/chitosan schiff base. *J. Mol. Struct.* **1321**, 139592 (2025).
- 8. Fernandes, C. M. et al. Selenocyanates and selenotetrazoles derivatives: A detailed experimental and theoretical evaluation as corrosion inhibitors for mild steel in aggressive environment. *Electrochim. Acta.* 475, 143629 (2024).
- Jafari, H., Ameri, E., Rezaeivala, M. & Berisha, A. Experimental and theoretical studies on protecting steel against 0.5 M H₂SO₄ corrosion by new schiff base. J. Indian Chem. Soc. 99, 100665 (2022).
- 10. Jafari, H., Ámeri, E., Vakili, M. H. & Berisha, A. Effect of OH position on adsorption behavior of Schiff-base derivatives in corrosion Inhibition of carbon steel in 1 M HCl. *Electrochem. Commun.* **159**, 107653 (2024).
- 11. Jafari, H., Akbarzade, K. & Danaee, I. Corrosion Inhibition of carbon steel immersed in a 1 M HCl solution using benzothiazole derivatives. *Arab. J. Chem.* 12, 1387–1394 (2019).
- 12. Jafari, H., Ameri, E., Vakili, M. H. & Berisha, A. Novel silicon-based schiff base as corrosion inhibitor for anti-corrosion behavior of API 5L grade B in 1 M HCl. *Mater. Chem. Phys.* 311, 128499 (2024).
- Jafari, H. & Ameri, E. Synthesis and evaluation of schiff base as corrosion inhibitor for carbon steel in 1 M HCl solution. Anti-Corros Methods Mater. 71, 632–639 (2024).
- 14. Jafari, H., Ameri, E., Rezaeivala, M., Berisha, A. & Halili, J. Anti-corrosion behavior of two N₂O₄ Schiff-base ligands: experimental and theoretical studies. *J. Phys. Chem. Solids.* **164**, 110645 (2022).
- and the local studies. J. Phys. Chem. Soluta. 104, 110045 (2022).

 15. Jawad, Q. A. et al. Synthesis, characterization, and corrosion Inhibition potential of novel thiosemicarbazone on mild steel in sulfuric acid environment. Coatings 9, 729 (2019).
- 16. Mansour, A. A. et al. Evaluation of N80 carbon steel corrosion in 15 wt.% HCl using isatin-hydrazones: A comprehensive
- approach with chemical, electrochemical techniques, and DFTB calculations. *J. Mol. Struct.* 1321, 139910 (2025).
 17. Mansour, A. A. et al. Investigating corrosion failure in N80 carbon steel: experimental and theoretical insights into Isonicotinohydrazide derivatives as inhibitors in acidic conditions. *Inorg. Chem. Commun.* 161, 112007 (2024).
- 18. Mansour, A. A. et al. Exploring the potential of Isonicotinohydrazide derivatives in N80 steel corrosion control: an integrated approach through synthesis, modeling, and experimentation in acidic environments. *Colloids Surf. Physicochem Eng. Asp.* 679, 132542 (2023).
- 19. Sheetal et al. Aromaticity of heterocyclic compounds and their corrosion Inhibition property: experimental and theoretical analysis. *Langmuir* 40, 21675–21692 (2024).
- 20. Sayed, A. G., Ashmawy, A. M., Elgammal, W. E., Hassan, S. M. & Deyab, M. A. Synthesis, description, and application of novel corrosion inhibitors for CS AISI1095 in 1.0 M HCl based on benzoquinoline derivatives. *Sci. Rep.* 13, 13761 (2023).
- 21. Toghan, A. et al. Effect of adsorption and interactions of new triazole-thione-Schiff bases on the corrosion rate of carbon steel in 1 M HCl solution: theoretical and experimental evaluation. ACS Omega. 9, 6761–6772 (2024).
- 22. Motawea, M. M. et al. Fabrication of protective organic layer using thiazolyl-pyrazolone compound as an efficient corrosion inhibitor for CS-N80 in 0.5 M H₂SO₄ solution. *J. Mol. Struct.* **1330**, 141469 (2025).
- 23. Alahiane, M. et al. Corrosion Inhibition of SS 316L by organic compounds: experimental, molecular dynamics, and conceptualization of molecules–surface bonding in H₂SO₄ solution. *Appl. Surf. Sci.* **612**, 155755 (2023).
- El Badaoui, H. et al. A comprehensive study on the corrosion Inhibition of N80 carbon steel by acetamide derivatives in a 3.5% NaCl corrosive medium utilizing electrochemical methods and the DFTB approach. J. Environ. Chem. Eng. 13, 116828 (2025).
- Jafari, H., Danaee, I., Eskandari, H. & RashvandAvei, M. Combined computational and experimental study on the adsorption and Inhibition effects of N₂O₂ schiff base on the corrosion of API 5L grade B steel in 1 mol/l HCl. J. Mater. Sci. Technol. 30, 239–252 (2014).
- 26. Jafari, H., Rezaeivala, M., Mokhtarian, N., Berisha, A. & Ameri, E. Corrosion Inhibition of carbon steel in 0.5 M H₂SO₄ by new reduced schiff base ligand. *J. Bio-Tribo-Corros.* **8**, 81 (2022).
- 27. Jafari, H., Ameri, E., Rezaeivala, M. & Berisha, A. 4,4'-(((2,2-dimethylpropane-1,3-diyl)bis(azanediyl)bis(methylene))bis(2-methoxyphenol)) as new reduced form of schiff base for protecting API 5L grade B in 1 M HCl. *Arab. J. Sci. Eng.* 48, 7359–7372 (2023)
- 28. Jafari, H., Ameri, E., Rezaeivala, M., Berisha, A. & Vakili, M. H. Comparison of the anticorrosion behavior of three symmetrical Schiff-base ligands: experimental and theoretical studies. *J. Appl. Electrochem.* **52**, 1803–1818 (2022).
- Rehioui, M. et al. 1,2,4-Triazole-5-thione derivative for inhibiting carbon steel corrosion in 1 M hcl: synthesis, electrochemical, SEM/EDX, DFT, and MD investigations. J. Mol. Struct. 1303, 137577 (2024).
- 30. Abdelli, A. et al. Recent advances in the chemistry of 1,2,4-triazoles: synthesis, reactivity and biological activities. *Tetrahedron Lett.* **86**, 153518 (2021).
- 31. Hazazi, O. A., Fawzy, A., Shaaban, M. R. & Awad, M. I. Enhanced 4-amino-5-methyl-4H-1,2,4-triazole-3-thiol Inhibition of corrosion of mild steel in 0.5 M H₂SO₄ by Cu(II). *Int. J. Electrochem. Sci.* 9, 1378–1389 (2014).
- 32. Elazhary, I. et al. Comparative study of 1,2,3-triazole derivatives as corrosion inhibitors of mild steel in sulphuric acid solution.

 *Anti-Corros Methods Mater. 66, 544–555 (2019).
- John, S. & Joseph, A. Electroanalytical studies of the corrosion-protection properties of 4-amino-4H-1,2,4-triazole-3,5-dimethanol (ATD) on mild steel in 0.5 N sulfuric acid. Res. Chem. Intermed. 38, 1359–1373 (2012).
- 34. Belal, K., El-Askalany, A., Ghaith, E. A. & Molouk, A. F. Novel synthesized Triazole derivatives as effective corrosion inhibitors for carbon steel in 1 M HCl solution: experimental and computational studies. *Sci. Rep.* 13, 22180 (2023).
- 35. Ashraf, A., Riaz, N., Muzaffar, S., Atif, M. & Bashir, B. Investigating the potential of 1,2,4-triazoles as corrosion inhibitors for copper and steel: A comprehensive review. *Next Res.* 1, 100033 (2024).
- 36. Swathi, N. P. et al. Investigation of some new Triazole derivatives for inhibiting the acid corrosion of C1018 carbon steel: correlation of electrochemical studies with quantum chemical calculations. S Afr. J. Chem. Eng. 44, 123–134 (2023).
- 37. Verma, C., Quraishi, M. A. & Ebenso, E. E. Quinoline and its derivatives as corrosion inhibitors: A review. Surf. Interfaces. 21, 100634 (2020).
- 38. Verma, C., Rhee, K. Y., Quraishi, M. A. & Ebenso, E. E. Pyridine-based N-heterocyclic compounds as aqueous phase corrosion inhibitors: A review. *J. Taiwan. Inst. Chem. Eng.* 117, 265–277 (2020).
- 39. Wang, J. et al. Frontiers and advances in N-heterocycle compounds as corrosion inhibitors in acid medium: recent advances. *Adv. Colloid Interface Sci.* **321**, 103031 (2023).
- 40. Daoudi, W. et al. Synthesis, characterization, and corrosion Inhibition activity of new imidazo[1.2-a]pyridine Chalcones. *Mater. Sci. Eng. B.* **290**, 116287 (2023).
- 41. Abdelshafi, N. S., Ibrahim, M. A., Badran, A. S. & Halim, S. A. Experimental and theoretical evaluation of a newly synthesized Quinoline derivative as corrosion inhibitor for iron in 1.0 M hydrochloric acid solution. *J. Mol. Struct.* **1250**, 131750 (2022).

- 42. Abd El-Maksoud, S. A. & Fouda, A. S. Some pyridine derivatives as corrosion inhibitors for carbon steel in acidic medium. *Mater. Chem. Phys.* **93**, 84–90 (2005).
- 43. Jafari, H., Mohsenifar, F. & Sayin, K. Corrosion Inhibition studies of N,N'-bis(4-formylphenol)-1,2-diaminocyclohexane on steel in 1 M HCl solution. J. Taiwan. Inst. Chem. Eng. 64, 314–324 (2016).
- Sayin, K., Jafari, H. & Mohsenifar, F. Effect of pyridyl on adsorption behavior and corrosion Inhibition of Aminotriazole. J. Taiwan. Inst. Chem. Eng. 68, 431–439 (2016).
- 45. El Basiony, N. et al. Synthesis, characterization, experimental and theoretical calculations (DFT and MC) of ethoxylated aminothiazole as inhibitor for X65 steel corrosion in highly aggressive acidic media. *J. Mol. Liq.* **297**, 111940 (2020).
- 46. Abd El-Lateef, H. M., Shalabi, K. & Tantawy, A. H. Corrosion Inhibition and adsorption features of novel bioactive cationic surfactants bearing benzenesulphonamide on C1018-steel under sweet conditions: combined modeling and experimental approaches. *J. Mol. Liq.* 320, 114564 (2020).
- 47. Al-Masoud, M. A., Khalaf, M. M., Mohamed, I. M., Shalabi, K. & Abd El-Lateef, H. M. Computational, kinetic, and electrochemical studies of polyaniline functionalized ZnO and ZnO–SiO₂ nanoparticles as corrosion protection films on carbon steel in acidic sodium chloride solutions. *J. Ind. Eng. Chem.* 112, 398–422 (2022).
- 48. Gouda, M., Khalaf, M. M., Shalabi, K., Al-Omair, M. A. & Abd El-Lateef, H. M. Synthesis and characterization of Zn-organic frameworks containing Chitosan as a low-cost inhibitor for sulfuric-acid-induced steel corrosion: practical and computational exploration. *Polymers* 14, 228 (2022).
- Shalabi, K., Helmy, A., El-Askalany, A. & Shahba, M. New pyridinium bromide mono-cationic surfactant as corrosion inhibitor for carbon steel during chemical cleaning: experimental and theoretical studies. J. Mol. Liq. 293, 111480 (2019).
- 50. Gapsari, F. et al. Efficacy of *Andrographis paniculata* leaf extract as a green corrosion inhibitor for mild steel in concentrated sulfuric acid: experimental and computational insights. *Results Surf. Interfaces.* 18, 100361 (2025).
- Abd El-Lateef, H. M., Shalabi, K. & Tantawy, A. H. Corrosion Inhibition of carbon steel in hydrochloric acid solution using newly synthesized urea-based cationic fluorosurfactants: experimental and computational investigations. New. J. Chem. 44, 17791– 17814 (2020).
- 52. Beniken, M. et al. Adsorption behavior and corrosion Inhibition mechanism of a polyacrylamide on C-steel in 0.5 M H₂SO₄: electrochemical assessments and molecular dynamic simulation. *J. Mol. Liq.* **348**, 118022 (2022).
- 53. Shaban, M. M. et al. Anti-corrosion, antiscalant and anti-microbial performance of some synthesized trimeric cationic imidazolium salts in oilfield applications. *J. Mol. Liq.* **351**, 118610 (2022).
- 54. EL-Haddad, M. N. & Fouda, A. Investigating *Xanthium spinosum* extract as an eco-friendly corrosion inhibitor for aluminium in acidic environments: A green approach to metal protection. *Results Chem.* 14, 102136 (2025).
- 55. Kamal, R. S., Migahed, M. A. & Abd El-Sattar, N. E. Synthesis, characterization and performance of succinimide derivatives as anti-corrosion and anti-scalant in petroleum applications. *J. Mol. Liq.* **354**, 118869 (2022).
- Nasser, A., Migahed, M., El Basiony, N., Abd-El-Bary, H. & Mohamed, T. A. Electrochemical, surface analysis, computational and anticorrosive studies of novel di-imine schiff base on X65 steel surface. Sci. Rep. 13, 10457 (2023).
- 57. Shaaban, S. et al. Novel organoselenides as efficient corrosion inhibitors for N80 steel in a 3.5 wt% sodium chloride solution. *Inorg. Chem. Commun.* 172, 113632 (2025).
- 58. Eid, A., Shaaban, S. & Shalabi, K. Tetrazole-based organoselenium bi-functionalized corrosion inhibitors during oil well acidizing: experimental, computational studies, and SRB bioassay. *J. Mol. Liq.* **298**, 111980 (2020).
- 59. Al Jahdaly, B. A. Electrochemical and DFT insights into 2-amino-4-(4-hydroxy-3-methoxyphenyl)-7-methyl-4H-chromene-3-carbonitrile: an innovative strategy for antibacterial activity and corrosion protection of carbon steel. *RSC Adv.* 14, 24039–24054
- 60. Abd El-Lateef, H. M., Khalaf, M. M., Shalabi, K. & Abdelhamid, A. A. Multicomponent synthesis and designing of tetrasubstituted imidazole compounds catalyzed via ionic-liquid for acid steel corrosion protection: experimental exploration and theoretical calculations. Chin. J. Chem. Eng. 55, 304–319 (2023).
- 61. Hsissou, R. et al. Insight of development of two cured epoxy polymer composite coatings as highly protective efficiency for carbon steel in sodium chloride solution: DFT, RDF, FFV and MD approaches. *J. Mol. Liq.* **360**, 119406 (2022).
- 62. Timothy, U. J. et al. In-situ biosynthesized plant exudate gums-silver nanocomposites as corrosion inhibitors for mild steel in hydrochloric acid medium. *Int. J. Biol. Macromol.* **269**, 132065 (2024).
- 63. Selim, Y. A. et al. An electrochemical and surface studies of synthesized gemini ionic liquid as corrosion inhibitor for carbon steel in petroleum field. Sci. Rep. 14, 10766 (2024).
- 64. Naciri, M. et al. Unveiling the influence of Furan and thiophene on the corrosion Inhibition capabilities of novel hydrazones derivatives in carbon steel/hcl interface: A dual experimental–theoretical study. *Colloids Surf. Physicochem Eng. Asp.* 686, 133272
- 65. Salim, M., Azab, M., Abo-Riya, M. A. & Abd-El-Raouf, M. El basiony, N. Controlling C-steel dissolution in 1 M HCl solution using newly synthesized ρ-substituted Imine derivatives: theoretical (DFT and MCs) and experimental investigations. J. Mol. Struct. 1274, 134357 (2023).
- 66. Elaraby, A., Qasim, K. F., Mohamed, S. K., El-Sharkawy, E. & Abdelhamed, S. Di-imine schiff base inhibitor for carbon steel corrosion in 1 M hcl: electrochemical, surface and theoretical investigations. *J. Environ. Chem. Eng.* 12, 111861 (2024).
- 67. Almashhadani, H. A., Alshujery, M. K., Khalil, M., Kadhem, M. M. & Khadom, A. A. Corrosion Inhibition behavior of expired diclofenac sodium drug for al 6061 alloy in aqueous media: electrochemical, morphological, and theoretical investigations. *J. Mol. Liq.* 343, 117656 (2021).
- El Faydy, M. et al. Corrosion Inhibition performance of newly synthesized 5-alkoxymethyl-8-hydroxyquinoline derivatives for carbon steel in 1 M HCl solution: experimental, DFT and Monte Carlo simulation studies. *Phys. Chem. Chem. Phys.* 20, 20167– 20187 (2018).
- Elaraby, A. et al. Synthesis of gemini cationic surfactants based on natural nicotinic acid and evaluation of their Inhibition performance at C-steel/1 M HCl interface: electrochemical and computational investigations. Colloids Surf. Physicochem Eng. Asp. 659, 130687 (2023).
- Shaban, S. M. et al. Corrosion Inhibition and surface examination of carbon steel 1018 via N-(2-(2-hydroxyethoxy)ethyl)-N,N-dimethyloctan-1-aminium bromide in 1.0 M HCl. J. Mol. Struct. 1227, 129713 (2021).
- 71. Kellal, R. et al. A sustainable approach exploiting *Chrysanthemum coronarium* flowers distillation waste as a corrosion suppressor for low carbon steel in monoprotic acid medium through electrochemical and computational evaluations. *Mater. Chem. Phys.* **314**, 128846 (2024).
- Raisemche, L. et al. Corrosion Inhibition of mild steel in acidic environments: mechanistic insights and protective effects of azocum inhibitor. J. Environ. Chem. Eng. 12, 112354 (2024).
- 73. Ismail, M. A. et al. Novel cationic Aryl bithiophene/terthiophene derivatives as corrosion inhibitors by chemical, electrochemical and surface investigations. Sci. Rep. 12, 3192 (2022).
- 74. En-Nyly, M. et al. Elucidating the mechanisms of novel thiazole-based corrosion inhibitors in carbon steel/hcl interface: an integrated approach combining experimental and computational studies. J. Mol. Struct. 1306, 137817 (2024).
- 75. Ech-Chihbi, E. et al. Experimental and computational studies on the Inhibition performance of the organic compound 2-phenylimidazo[1,2-a]pyrimidine-3-carbaldehyde against the corrosion of carbon steel in 1.0 M HCl solution. *Surf. Interfaces.* 9, 206–217 (2017).

- 76. Alharbi, B. et al. Synthesis and investigation of two new compounds (2-(methoxymethyl)-1-phenyl-2-propen-1-one and 2-(methoxymethyl)-1-(4-methoxyphenyl)-2-propen-1-one) as corrosion inhibitors for mild steel in acidic solutions at elevated temperature. *Int. J. Electrochem. Sci.* **19**, 100508 (2024).
- 77. Yıldız, R. An electrochemical and theoretical evaluation of 4,6-diamino-2-pyrimidinethiol as a corrosion inhibitor for mild steel in HCl solutions. *Corros. Sci.* **90**, 544–553 (2015).
- 78. Yadav, M., Gope, L. & Sarkar, T. K. Synthesized amino acid compounds as eco-friendly corrosion inhibitors for mild steel in hydrochloric acid solution: electrochemical and quantum studies. *Res. Chem. Intermed.* 42, 2641–2660 (2016).
- 79. Ouakki, M. et al. A detailed investigation on the corrosion Inhibition effect of by newly synthesized Pyran derivative on mild steel in 1.0 M hcl: experimental, surface morphological (SEM-EDS, DRX & AFM) and computational analysis (DFT & MD simulation). *J. Mol. Liq.* **344**, 117777 (2021).
- 80. Eissa, M. E., Etaiw, S. H., El-Hussieny, E. S., ElHossiany, A. A. & Fouda, A. E.-A. S. Sweet orange Peel extract as green sustainable corrosion inhibitor for al in 1 M HCl. *Int. J. Electrochem. Sci.* 20, 100882 (2025).
- 81. Banu, A. M., Thakur, A., Farzana, B. A., Ahamed, F. M. & Kumar, A. Exploring the bio-inspired corrosion Inhibition properties of eco-friendly *Limonia acidissima* leaves extract for mild steel in acidic media: computational, electrochemical and spectroscopic insights. *J. Mol. Struct.* 1323, 140713 (2025).
- 82. Lakikza, I. et al. Unraveling the corrosion inhibition mechanisms of Algerian *Dryopteris filix-mas* leaf extract on A210C carbon steel in 1 M HCl: Comprehensive insights from electrochemical, morphological, XPS, and theoretical analyses. *Mater. Today Commun.* 42, 111262 (2025).
- 83. Zheng, T. et al. Synergistic corrosion Inhibition effects of quaternary ammonium salt cationic surfactants and thiourea on Q235 steel in sulfuric acid: experimental and theoretical research. *Corros. Sci.* 199, 110199 (2022).
- 84. Alamry, K. A., Aslam, R., Khan, A., Hussein, M. A. & Tashkandi, N. Y. Evaluation of corrosion Inhibition performance of thiazolidine-2,4-diones and its amino derivative: gravimetric, electrochemical, spectroscopic, and surface morphological studies. *Process. Saf. Environ. Prot.* 159, 178–197 (2022).
- 85. Khamaysa, O. M. A. et al. Hydrazone-based green corrosion inhibitors for API grade carbon steel in hcl: insights from electrochemical, XPS, and computational studies. *Colloids Surf. Physicochem Eng. Asp.* 626, 127047 (2021).
- 86. Keshar, K. et al. Corrosion Inhibition and adsorption behaviour of benzothiazole compounds on mild steel in an acidic environment: experimental and theoretical approach. *Colloids Surf. Physicochem Eng. Asp.* 711, 136318 (2025).
- 87. Mehta, R. K., Yadav, M. & Obot, I. B. Electrochemical and computational investigation of adsorption and corrosion Inhibition behaviour of 2-aminobenzohydrazide derivatives at mild steel surface in 15% HCl. *Mater. Chem. Phys.* **290**, 126666 (2022).
- 88. Asfour, H., Elewady, G. Y., Zaki, E. G., Fouda, A. & E.-A. Synthesis and characterization of new polymeric ionic liquids as corrosion inhibitors for carbon steel in a corrosive medium: experimental, spectral, and theoretical studies. ACS Omega. 8, 41077–41099 (2023).
- 89. Abd, E., Maksoud, S., Fouda, A. E. A. & Badawy, H. Furosemide drug as a corrosion inhibitor for carbon steel in 1.0 M hydrochloric acid. Sci. Rep. 14, 9052 (2024).
- 90. Fouda, A. E. A. S., Etaiw, S. E. H., Ismail, M. A., El-Aziz, A., Eladl, M. M. & D. M. & Experimental and computational approaches of methoxy naphthylbithiophene derivatives and their use as corrosion protection for carbon steel in acidic medium. *Sci. Rep.* 13, 8712 (2023).
- 91. Sehmi, A. et al. Corrosion Inhibition of mild steel by newly synthesized pyrazole Carboxamide derivatives in HCl acid medium: experimental and theoretical studies. *J. Electrochem. Soc.* **167**, 155508 (2020).
- 92. Yadav, M., Kumar, S., Bahadur, I. & Ramjugernath, D. Corrosion inhibitive effect of synthesized thiourea derivatives on mild steel in a 15% HCl solution. *Int. J. Electrochem. Sci.* **9**, 6529–6550 (2014).
- 93. Abdou, M. M. & EL-Haddad, M. N. Novel eco-friendly Quinolinone derivative as a water-soluble corrosion inhibitor for low carbon steel: synthesis, inhibitive efficacy, and DFT analysis. *J. Mol. Struct.* 1324, 140889 (2025).
- 94. Luna, M. C. et al. Study of corrosion behavior of API 5L X52 steel in sulfuric acid in the presence of ionic liquid 1-ethyl 3-methylimidazolium thiocyanate as corrosion inhibitor. *J. Mol. Liq.* **289**, 111106 (2019).
- 95. Shalabi, K., El-Lateef, A., Hammouda, H. M., Tantawy, A. H. & M. M. & Synthesis and evaluation of anticorrosive properties of cationic benzenesulphonamide surfactants on carbon steel under sweet conditions: empirical and computational investigations. *J. Mol. Liq.* 415, 126363 (2024).
- 96. Shalabi, K., El-Lateef, A., Hammouda, H. M., Rashed, M. M. & M. M. & The anticorrosive efficacy of newly synthesized pyridobis(benzo [b] azoninone) analogs on carbon steel under sweet corrosive environments: A combined empirical and theoretical approaches. *Colloids Surf. Physicochem Eng. Asp.* **702**, 134958 (2024).
- Palaniappan, N., Cole, I. & Kuznetsov, A. Experimental and computational studies of graphene oxide covalently functionalized by octylamine: electrochemical stability, hydrogen evolution, and corrosion Inhibition of the AZ13 Mg alloy in 3.5% NaCl. RSC Adv. 10, 11426–11434 (2020).
- 98. Shalabi, K., El-Lateef, A., Hammouda, H. M., Abdelhamid, A. A. & M. M. & Green synthesizing and corrosion Inhibition characteristics of Azo compounds on carbon steel under sweet conditions: experimental and theoretical approaches. *ACS Omega.* **9**, 18932–18945 (2024).
- Yousif, Q. A., Nazeer, A., Fadel, A., Al-Hajji, Z., Shalabi, K. & L. A. & Design of new ecofriendly schiff base inhibitors for carbon steel corrosion protection in acidic solutions: electrochemical, surface, and theoretical studies. ACS Omega. 9, 14153–14173 (2024).
- 100. Abd El-Lateef, H. M. et al. Novel water-soluble organoselenocyanates and symmetrical diselenides tethered N-succinanilate and N-maleanilate as corrosion inhibitors for reinforced steel in the simulated concrete pore solution. Constr. Build. Mater. 366, 130135 (2023).
- 101. El-Gammal, O. A., Saad, D. A., El-Nahass, M. N., Shalabi, K. & Abdallah, Y. M. Bishydrazone ligand and its Zn-complex: synthesis, characterization and Estimation of scalability Inhibition mitigation effectiveness for API 5L X70 carbon steel in 3.5% NaCl solutions. RSC Adv. 14, 13258–13276 (2024).
- 102. Zgueni, H. et al. Theoretical and experimental study of the corrosion Inhibition of carbon steel in 1 M HCl solution by a new synthesized organic compound derived from carbendazim. *J. Mol. Struct.* **1327**, 141230 (2025).
- 103. Abdallah, Y., El-Gammal, O. A., El-Lateef, A., Shalabi, K. & H. M. & Synthesis and characterization of novel Dicarbohydrazide derivatives with electrochemical and theoretical approaches as potential corrosion inhibitors for N80 steel in a 3.5% NaCl solution. RSC Adv. 12, 14665–14685 (2022).
- 104. El-Saeed, H. et al. Synthesis and characterization of novel ionic liquids based on imidazolium for acid corrosion Inhibition of aluminum: experimental, spectral, and computational study. J. Mol. Liq. 358, 119177 (2022).
- 105. Sattari, R., Khayati, G. R. & Darezereshki, E. Study of anti-corrosion properties of ellagic acid and Curcumin derived from plants in saline medium: experimental, quantum chemical, Monte Carlo and molecular dynamic simulation. *Colloids Surf. Physicochem Eng. Asp.* 711, 136349 (2025).
- 106. Ramezanzadeh, M., Bahlakeh, G. & Ramezanzadeh, B. Study of the synergistic effect of Mangifera indica leaves extract and zinc ions on the mild steel corrosion Inhibition in simulated seawater: computational and electrochemical studies. J. Mol. Liq. 292, 111387 (2019).
- 107. Goyal, M., Kumar, S., Guo, L., Alrefaee, S. H. & Verma, C. Influence of ring size on corrosion Inhibition potential of environmental sustainable Cycloalkyltriphenylphosphonium based ionic liquids: computational and experimental demonstrations. *J. Taiwan. Inst. Chem. Eng.* 123, 21–33 (2021).

- 108. Khalaf, M. M., Gouda, M., Shalabi, K., Shaaban, S. & Abd El-Lateef, H. M. Structural and adsorptive characteristics of 2D multilayer nanoflakes of NiCo phosphates for chromium (VI) removal: experimental and Monte Carlo simulations. ACS Omega. 7, 10738–10750 (2022).
- 109. Abd El-Lateef, H. M., Shaaban, S., Khalaf, M. M., Toghan, A. & Shalabi, K. Synthesis, experimental, and computational studies of water soluble anthranilic organoselenium compounds as safe corrosion inhibitors for J55 pipeline steel in acidic oilfield formation water. Colloids Surf. Physicochem Eng. Asp. 625, 126894 (2021).
- Shaaban, S. et al. Diorganyl diselenide hybrids as effective corrosion inhibitors for carbon steel in HCl solution. J. Indian Chem. Soc. 102, 101794 (2025).
- 111. Jafari, H. & Sayin, K. Electrochemical and theoretical studies of adsorption and corrosion Inhibition of aniline Violet compound on carbon steel in acidic solution. *J. Taiwan. Inst. Chem. Eng.* **56**, 181–190 (2015).
- 112. Haruna, K. & Saleh, T. A. Dopamine functionalized graphene oxide (DGO) as a corrosion inhibitor against X60 carbon steel corrosion in a simulated acidizing environment; an electrochemical, weight loss, SERS, and computational study. Surf. Interfaces. 44, 103688 (2024).
- 113. Rouifi, Z. et al. Performance and computational studies of new soluble Triazole as corrosion inhibitor for carbon steel in HCl. *Chem. Data Collect.* **22**, 100242 (2019).
- 114. Murmu, M. et al. Corrosion Inhibition property of azomethine functionalized Triazole derivatives in 1 mol L⁻¹ HCl medium for mild steel: experimental and theoretical exploration. *J. Mol. Liq.* **313**, 113508 (2020).
- 115. Ahmad, Y. H., Mogoda, A. S. & Gadallh, A. G. Investigation of the inhibiting effect of some Triazole derivatives for the corrosion of mild steel in 1 M H₂SO₄ solution. *Int. J. Electrochem. Sci.* 7, 4929–4941 (2012).
- 116. Rouifi, Z. et al. 8-Hydroxyquinoline grafted Triazole derivatives as corrosion inhibitors for carbon steel in H₂SO₄ solution: electrochemical and theoretical studies. *Ionics* **27**, 2267–2288 (2021).
- 117. El Aoufir, Y. et al. The effect of the alkyl chain length on corrosion Inhibition performances of 1,2,4-triazole-based compounds for mild steel in 1.0 M hcl: insights from experimental and theoretical studies. *J. Mol. Liq.* 303, 112631 (2020).
- 118. Arshad, N., Akram, M., Altaf, F. & Yaqub, A. Anti-corrosive potentials of 1,2,4-triazole-5-thiones for mild steel 1030 in acidic environment. *Prot. Met. Phys. Chem. Surf.* **56**, 816–825 (2020).
- 119. Abdelsalam, M. M. et al. Green synthesis, electrochemical, and DFT studies on the corrosion Inhibition of steel by some novel Triazole schiff base derivatives in hydrochloric acid solution. *Arab. J. Chem.* 15, 103491 (2022).
- 120. Quraishi, M. A., Sudheer, Ansari, K. R. & Ebenso, E. E. 3-Aryl substituted Triazole derivatives as new and effective corrosion inhibitors for mild steel in hydrochloric acid solution. *Int. J. Electrochem. Sci.* 7, 7476–7492 (2012).

Acknowledgements

All authors express their deep thanks to the Egyptian Knowledge Bank, STDF (38313) and Springer Nature for the publishing agreement.

Author contributions

Kamelia Belal carried out the experimental work and wrote the manuscript. A.H. El-Askalany supervision, investigation, and methodology. Eslam A Ghaith contributed to synthesizing and characterizing the tested new compounds. Ahmed Fathi Salem Molouk supervised, participated in experimental work, and analyzed the data. All authors reviewed the manuscript.

Funding

Open access funding provided by The Science, Technology & Innovation Funding Authority (STDF) in cooperation with The Egyptian Knowledge Bank (EKB).

Declarations

Competing interests

The authors declare no competing interests.

Additional information

Supplementary Information The online version contains supplementary material available at https://doi.org/10.1038/s41598-025-10619-5.

Correspondence and requests for materials should be addressed to A.F.S.M.

Reprints and permissions information is available at www.nature.com/reprints.

Publisher's note Springer Nature remains neutral with regard to jurisdictional claims in published maps and institutional affiliations.

Open Access This article is licensed under a Creative Commons Attribution 4.0 International License, which permits use, sharing, adaptation, distribution and reproduction in any medium or format, as long as you give appropriate credit to the original author(s) and the source, provide a link to the Creative Commons licence, and indicate if changes were made. The images or other third party material in this article are included in the article's Creative Commons licence, unless indicated otherwise in a credit line to the material. If material is not included in the article's Creative Commons licence and your intended use is not permitted by statutory regulation or exceeds the permitted use, you will need to obtain permission directly from the copyright holder. To view a copy of this licence, visit https://creativecommons.org/licenses/by/4.0/.

© The Author(s) 2025